https://dx.doi.org/10.1016/j.buildenv.2023.111066
This is the Pre-Published Version.

Characteristics of droplets emission immediately around mouth during dental treatments

Chaojie Xing [a, b], Zhengtao Ai [a, b, *], Zhiwei Liu [c], Cheuk Ming Mak [d], Hai Ming Wong [e]

a Department of Civil Engineering, Hunan University, Changsha, 410082, China

b National Center for International Research Collaboration in Building Safety and Environment, Hunan University, Changsha, Hunan, China

c School of Civil Engineering, Central South University, Changsha, China

d Department of Building Services Engineering, The Hong Kong Polytechnic University, Hung Hom, Hong Kong, China

e Faculty of Dentistry, The University of Hong Kong, Pok Fu Lam, Hong Kong Island, Hong Kong, China

Chaojie Xing (chaojiexing@hnu.edu.cn);
Zhengtao Ai (zhengtaoai@hnu.edu.cn) (Corresponding author);
Zhiwei Liu (214801021@csu.edu.cn);
Cheuk Ming Mak (cheuk-ming.mak@polyu.edu.hk);
Hai Ming Wong (wonghmg@hku.hk)

Abstract: Spatial and temporal distribution of droplets emitted during dental treatments have been attracted increasing attention, but the emission characteristics of droplets around the source (namely, the mouth) have still not been fully understood. The present study investigated experimentally the emission characteristics of droplets around mouth during typical dental treatments. A manikin being treated by portable dental instruments simulated the dental treatments, while the laser light scattering technique and particle image velocimetry (PIV) technique were employed to perform the measurements. The peak mass fraction of droplets occurs around the droplet size from 20 μm to 40 μm, while the mass fraction of droplets with the diameter less than 100 μm accounts for over 80%. By fitting with the Rosin-Rammler equation, the mean size of droplets ($\bar{d}$) and the size distribution parameter (n) are 54.96 and 1.35, respectively. The dominant emission direction of droplets is towards the chest and the region above the chest. The emitted droplets formed approximately a cone shape, and its angle varied from 37° to 71° for different conditions. The maximum velocity of droplets at the location near the dummy's mouth exceeds 1.0 m/s for most conditions. The injecting flow rate and treated tooth position are the major factors influencing the emission direction, angle, and velocity. The detailed boundary conditions for droplets distribution and emission velocities are tabulated in detail. It is expected that the results can further increase our understanding of emission characteristics of droplets and provide accurate initial conditions for CFD simulations.

Keywords: Droplets; Powder-jet-handpieces; Ultrasonic scaling instrument; Laser light scattering; Particle image velocimetry

1 Introduction

© 2023. This manuscript version is made available under the CC-BY-NC-ND 4.0 license http://creativecommons.org/licenses/by-nc-nd/4.0/

During dental treatments, splatters with high momentum containing saliva, blood, teeth fragments, and calculus are generated with the use of instruments such as powder-jet-handpieces, ultrasonic scaling instrument, and high-speed air turbine handpieces. Some studies have shown that splatters may also contain metals such as silver, barium, zirconium, strontium, and ytterbium [1-2]. Excessive inhalation of these splatters can cause lung inflammation and increase the risk of lung cancer [3]. In addition, high loads of the SARS-COV-2 virus have been detected in the saliva of both symptomatic [4-5] and asymptomatic COVID-19 patients [6-7]. Pathogens have also been found in the blood of patients infected with Hepatitis B and Acquired Immunodeficiency Syndrome [8]. Splatters generated from patients with infectious diseases during dental treatments would cause risks to medical workers. From the perspective of disease transmission, there are two main ways for splatters to contact with healthy people in the treatment environment. Firstly, large droplets settle down to the patients' surrounding surfaces due to the gravitational effect [9-10], causing contact transmission. Secondly, small droplets, namely aerosols, suspend in the air for a long time, which could eventually deposit onto the eye tissue or be inhaled, causing airborne transmission [11-12]. Obviously, there is a strong need to understand the emission characteristics of droplet during dental treatments and then to develop effective control measures.

Existing control measures of the transmission of the splatters to a susceptible people can be divided into three categories: namely, source control, transmission route control (mainly referring to airborne route), and susceptible people protection. Source control measures include mainly mouthwash, rubber dam, low-volume suction, and high-volume suction [13-14]. The measures aiming for blocking the airborne transmission route are basically ventilation dilution and air cleaning [15]. In terms of susceptible people protection, personal protective equipment is widely used, such as protective clothing, face shield, and face mask. Even though a combination of measures were used, it was widely reported that the bacterial concentration in the clinic was higher than the recommended limit value of 500 CFU/m^3 [16-17]. In this regard, new effective control measures are still required. One of the basic prerequisites of developing effective control measures is the accurate understanding of the emission characteristics of droplets generated during dental treatments. Particularly for using CFD methods, such emission characteristics are fundamental initial boundary conditions.

The distribution of the emitted droplets in dental offices during dental treatments has been extensively investigated in past studies, mainly using tracer gas/particle and bacterial culture methods. Based on the sedimentation conditions of the tracer on the surfaces, it was found that the main contaminated area was within 1 m away from the patient's mouth [18-20]. The bacterial culture method led to a similar conclusion [21-22]. In terms of suspended aerosols, Xing et al. [23] and Polednik et al. [24] used aerosol collectors, such as aerosol-generating procedures (AGPs), to measure the spatiotemporal concentration distribution of aerosols around the patient's mouth during dental treatments, and found that the concentration of PM10.0 within 1.0 m away from the patient's mouth exceeded the recommended limit value of 150 μg/m^3 [25].

There were some studies on emission characteristics of droplets (mainly including size distribution and velocity) immediately near the mouth. Particle image velocimetry

(PIV) [26], optical flow tracking velocimetry (OFTV) [27], shadowgraphy technique (ST) [27-28], digital inline holography (DIH), laser sheet imaging (LSI) [29], and tracer gas/particle method [30] were used to measure these characteristics based on dummy. However, these studies focused on limited scenarios, such as during maxillary and mandibular incisors and the use of ultrasonic scaling instrument [26-27,29] and did not reveal the complete emission characteristics, including the emission angle, speed, scope and the distribution of emitted droplets. In addition, regarding treatment procedures, the past studies mostly focused on the scenarios of using ultrasonic scaling, with little attention paid to air-powder-polishing that is an important procedure during teeth cleaning. To further understand the characteristics of droplets emission immediately around the mouth during the use of powder-jet-handpieces and ultrasonic scaling instruments, both the spray size measurement and the PIV measurement were performed. The influence of the applying amount of artificial saliva, treatment tooth position, and flow rate of the instruments, on the size distribution of emitted droplets, and the emission velocity and emission angle of the droplets around the mouth was investigated. The results should increase our understanding of the emission characteristics of droplets around mouth and provide more accurate and reliable initial boundary conditions for CFD simulations, which then would contribute to improved control measures.

2 Experimental methods

2.1 Experimental setups

The teaching dummy model, representing patient, used in the Stomatological School, which was highly identical to human mouth, was selected to perform the simulated dental treatments. As shown in Figure 1, the dummy has its head and half of the body, which had a detailed and accurate geometry of the mouth and cavity. The material of the dummy's teeth was ceramics, and the gingiva and lips were made of soft rubber. The mouth was fully opened.

In Figure 1, portable dental treatment instruments were selected to perform the treatments. This instrument included powder-jet-handpieces, ultrasonic scaling instrument, high-volume suction system, low-volume suction system, high-speed air turbine handpiece, and so on, which can be used for common dental treatments. The function of the powder-jet-handpieces was to eliminate the pigment on the teeth surfaces. During the treatments, the generated splatters, with high momentum, carrying pollutants on the teeth surfaces emitted into the surrounding air. In this study, the droplets were released from powder-jet-handpieces and then impacted the teeth surface. In the end, some droplets settled into the mouth and the others emitted into the air. The function of the ultrasonic scaling instrument was to eliminate teeth calculus through ultrasonic vibration, and the main reason for its splatters is that the coolant with a certain momentum impacting the teeth surface and emitted back to the air. The ultrasonic scaling instrument used in this study had a vibration frequency of 30 kHz. The flow rate was adjusted by the rotary control button during the use of the powder-jet-handpieces or ultrasonic scaling instrument. Meanwhile, the instruments were fixed with brackets to prevent from moving.

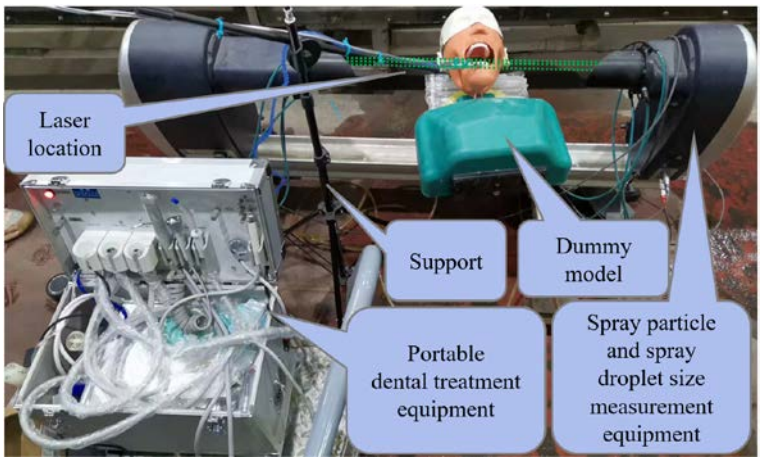

Figure 1 The droplet size measurement system.

2.2 Experimental instruments

The droplets size and emission characteristics were measured in a windless environment with air temperatures of 8.8-15.4 °C and 16.1-17.8 °C, and relative humidity of 26.7-49.5 % and 48.5-62.3 %, respectively.

Figure 1 shows the droplet size measurement system, where the laser light scattering technique measures first the intensity of the scattered light when the droplets pass the laser beam and then calculates the droplets size with the predefined code. The parameters of the instrument were listed in Table 1. The measurable particle size range of the instrument was between 2 μm and 2000 μm, which was suitable for the present study. To avoid the influence of evaporation on the droplet size distribution as much as possible, the dummy's mouth and thus the treatment teeth (namely, the source of the emission) were placed close to the laser beam. This measurement system provided the real-time measurement data. In addition, to reduce measurement errors, the system was calibrated before each measurement.

Table 1 The general parameters of the droplet size measurement system.

Overall	Parameters sizes/Methods
Analysis	Mie and Fraunhofer scattering including a patented multiple scattering analysis.
Data acquisition rate	Rapid mode: 10 kHz. Continuous mode: 1 Hz.
Maximum Measurement Time	Rapid mode: 30 seconds. Continuous mode: 60 minutes.
Droplets size	2 – 2000 μm
Accuracy	Better than 1%.
Repeatability	Better than 1%.
Reproducibility	Better than 1%.

PIV system was used to study the flow-field characteristics of droplets near the dummy's mouth, which has well demonstrated advantages in the measurement of the

velocity of particles [31]. As shown in Figure 2, the measurement platform included Nd: YAG double pulse laser, synchronizer, and high-speed CMOS camera, and the details were presented in Table 2. The droplets released by the dental instruments, including powder-jet-handpieces and ultrasonic scaling instrument, in the present study have good visualization performance. Therefore, there was no need to add additional tracer particles. Meanwhile, the error caused by the uneven spread of tracer particles can be avoided [32].

During the arrangement of the instrument, the laser from a double-pulse laser (380 MJ/pulse) illuminated the measurement plane. A high-speed camera for collecting droplets information (resolution: 2560 × 2160 $Pixel^2$, Model: Hisense Zyla CMOS) was directly placed opposite the measurement plane, as shown in Figure 2. To avoid measurement errors, the distance between the high-speed camera and the plane was determined after position calibration. The maximum view area of this system was 0.423 × 0.356 m^2.

The time interval between the double pulses influences the accuracy of results. It was determined to be 1.0 ms after some trial measurements, which met the standards proposed by Boillot and Prasad [33]. Data acquisition was achieved by Dynamic Studio v5.1 that was the software of this PIV system. During data processing, the velocity vector was obtained by adaptive PIV method that was the method used for data processing of software. The measurement error of PIV, including statistical and systematic error, was less than 3.5 % [31].

Table 2 PIV system measurement parameters.

Overall	Key parameters	Sizes/Type
Basic setting	Sampling frequency	5 Hz
	Sampling quantity	200
	Field of view	0.4 × 0.4 m^2
Algorithms	Adaptive PIV with high precision sub-pixel interpolation scheme	
	Size of interrogation area	64 × 64 $pixel^2$
	Overlap of interrogation area	50%
	Processing software	Dynamic Studio v5.1
Laser	Laser source	Double cavity Nd: YAG laser
	Laser power	380 MJ/pulse
	Thickness	1 mm
	Time between pulses	1 ms
Camera	Camera model	Hisense Zyla CMOS camera
	Resolution	2560 × 2160 $pixel^2$

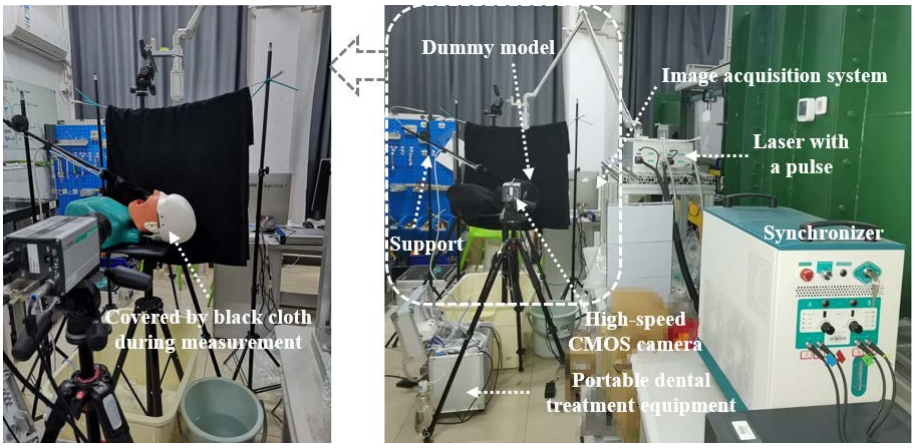

Figure 2 PIV measurement system of the flow-field characteristics of emitted droplets during dental treatments

2.3 Experimental conditions

During the real-life dental treatments, the amount of saliva existed on the teeth surface, the flow rate of the instruments, and the position of the treated teeth change over time. To study the influence of these variables on the droplets size distribution and flow-field characteristics of droplets, 7 cases were designed for the condition during the use of powder-jet-handpieces and ultrasonic scaling instrument, as shown in Table 3. The position of teeth is shown in Figure 3. For Cases 1-2, no artificial saliva was used in Case 1, and 2 ml artificial saliva was used in Case 2 to wet the treated teeth before measurements. The main ingredients of artificial saliva included NaCl, KCl, Urea, and pure water. The pH value of the artificial saliva was 6.8 and its viscosity was 4.52 mPa.s. For Cases 3-7, before the measurements, 2 ml artificial saliva was applied to wet the treated teeth. The only difference between Cases 2, 3, and 4 was the flow rates of the instruments, which represented medium flow rate, low flow rate, and high flow rate during dental treatments. Cases 1-4 corresponded to the maxillary incisors, as shown in Figure 4(a) and Figure 5(a). To study the influence of the obstruction of lip and surrounding soft tissue on tooth treatment at different positions, Cases 2, 5, 6, and 7 were set up, which corresponded to maxillary incisors, maxillary side teeth, mandibular incisors, and mandibular side teeth, as shown in Figure 4 (a)-(d) and Figure 5 (a)-(d). In terms of using methods of the instruments, the powder-jet-handpieces were used along the direction from the gums towards the mouth; the angles with the teeth surface were from 30° to 60°; and the distances from teeth surface were 3-5 mm. The handle of the ultrasonic scaling instrument was approximately vertical to the teeth surface, and its end attached snugly with the teeth surface or gap. It should be noted that these treatment methods were highly identical with those in practice.

Table 3 Details of experimental conditions; the position of teeth can be found in Figure 3.

Cases	Artificial saliva(ml)	Flow rate of Powder-jet-handpieces /Ultrasonic scaling instrument	The position of teeth treated during measurement

		(ml/min)	
1	0	60/30	9th/Between 8th and 9th
2	2	60/30	9th /Between 8th and 9th
3	2	40/15	9th /Between 8th and 9th
4	2	80/50	9th /Between 8th and 9th
5	2	60/30	12th /Between 5th and 6th
6	2	60/30	24th /Between 24th and 25th
7	2	60/30	21st /Between 27th and 28th

For droplet size, the measurement duration of each case was 5 min, and the data recording interval was 1 s. It was discovered that the emissions were mainly towards the directions of the dummy's head and chest. Therefore, the vertical plane at the center of the mouth along the direction of the dummy's head and chest was used as the main measured plane. As shown in Figure 4(a) and Figure 5(a), to study the influence of different measurement planes on the results, the measurement planes through the P2/G2 (teeth edge) and P1/G1 (middle) lines were also added for analysis. Each case was continuously measured for 40 s at a sampling frequency of 5 Hz, leading to 200 samples. To allow droplets generated during a previous measurement to settle or dilute sufficiently, the time interval between two continuous measurements was 30 minutes.

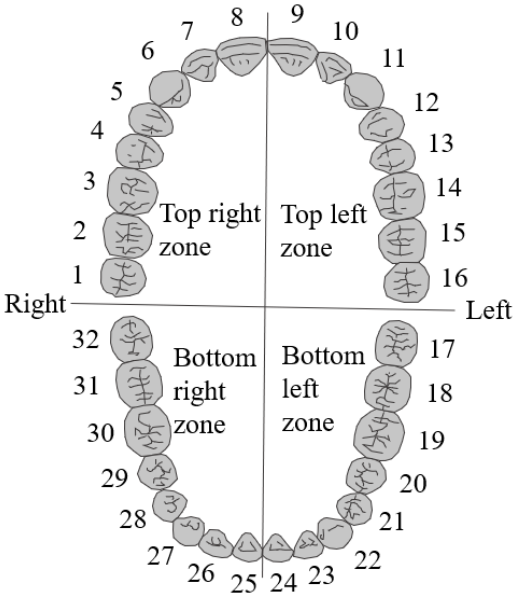

Figure 3 Teeth distribution and tooth number

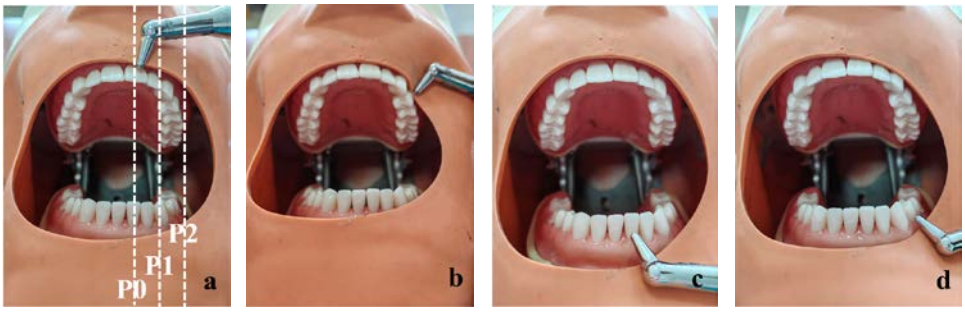

Figure 4 Location of the treatments with powder-jet-handpieces: (a) the tooth No. 9, (b) the tooth No. 12, (c) the tooth No. 24, and (d) the tooth No. 21.

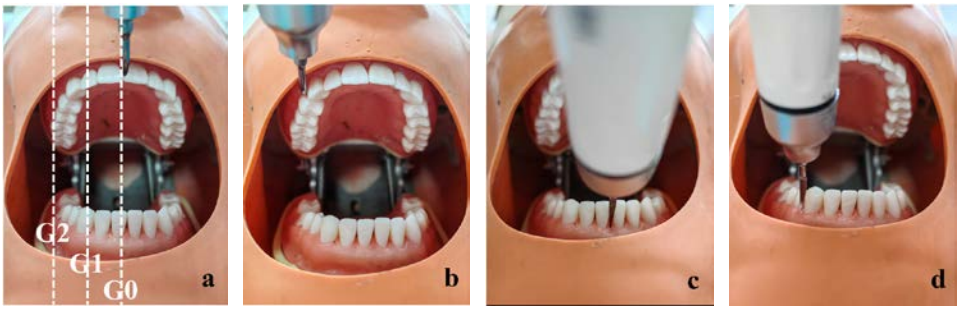

Figure 5 Location of the treatments with ultrasonic scaling instrument: (a) between the teeth No. 8 and 9, (b) between the teeth No. 5 and 6, (c) between the teeth No. 24 and 25, and (d) between the teeth No. 27 and 28.

3 Results and analyses

The analysis methods of droplets generated during the use of the air-powder-polishing and ultrasonic scaling are the same, and the results obtained with the two instruments did not differ obviously. Therefore, the following analysis was based on the process of air-powder-polishing, and results related to ultrasonic scaling were presented in the Appendix.

3.1 Size distribution of droplets

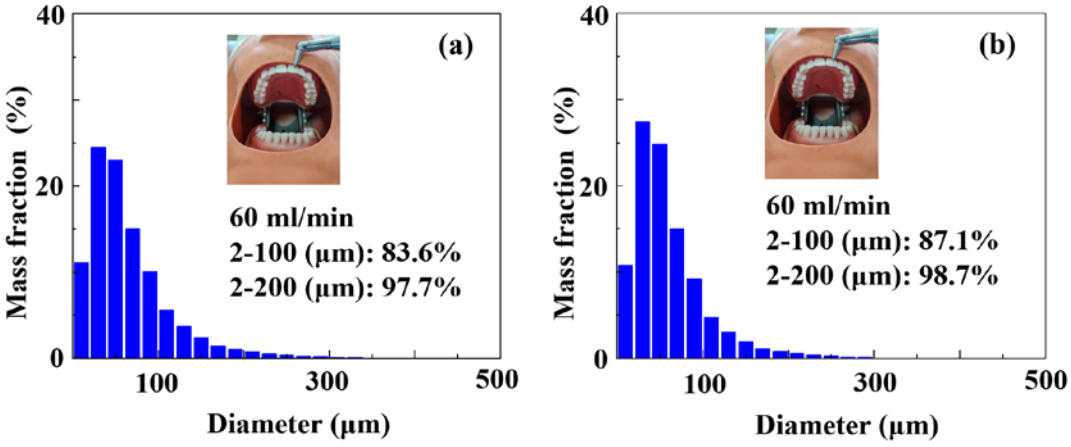

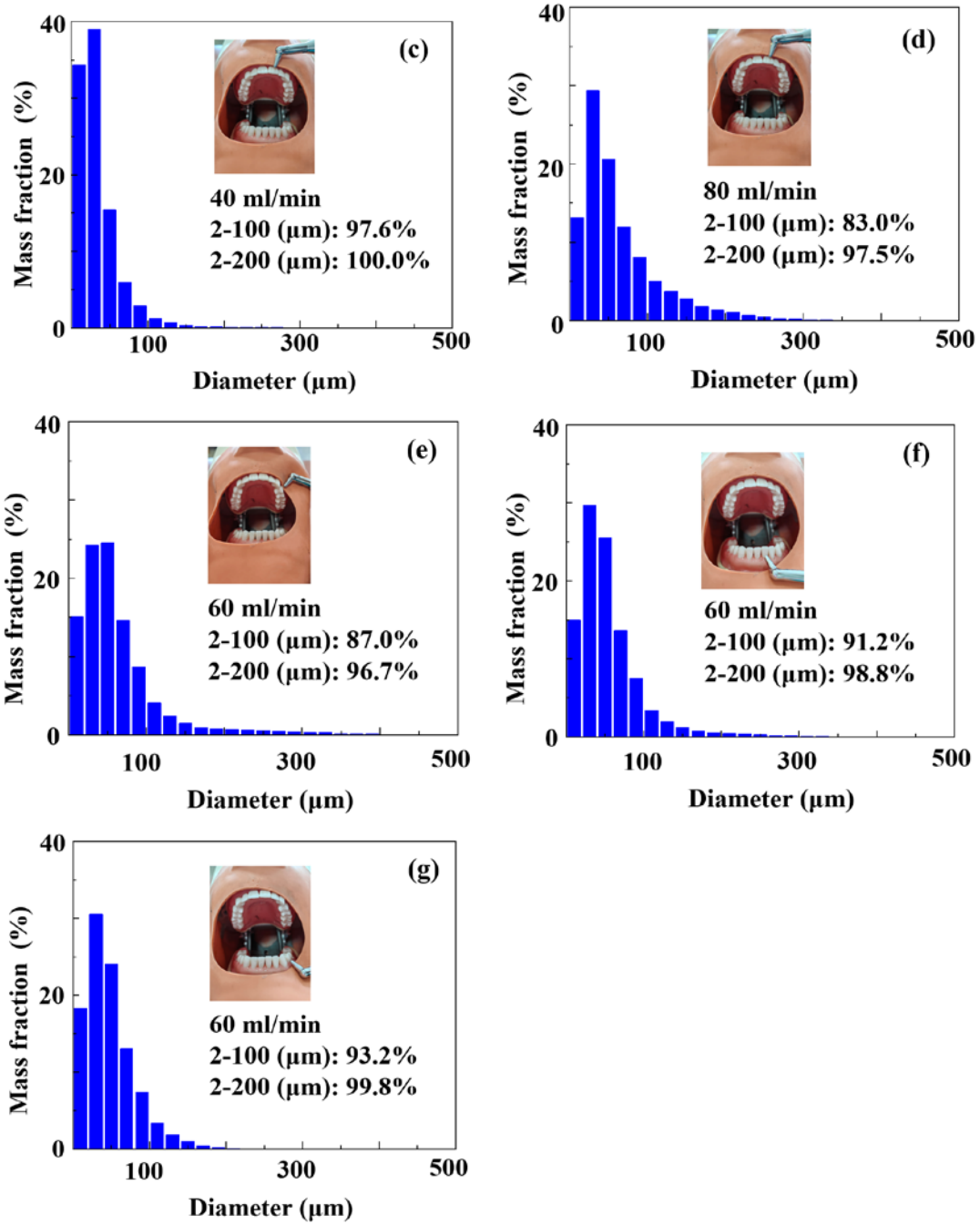

Figure 6 The mass fraction distribution of droplets size during the process of air-powder-polishing: (a)-(g) corresponding to Cases 1-7, where the flow rate and the percentages of mass for certain range of droplets are presented

Figure 6 presents the mass fraction distribution of droplets during the treatment using air-powder-polishing and the Table 4 lists the values. It can be observed that the peak mass fraction occurred around the droplet size from 20 μm to 40 μm. In addition, for all cases, the mass fraction of droplets in the range of 2-100 μm, 2-200 μm, and 2-300 μm, were more than 83.0%, 96.7%, and 99.3%, respectively. Apart from these general observations, the following analysis of the influential factors can be made.

Figure 6 (a) and (b) shows that the saliva had a little influence on the droplets size

distribution, which should be attributed to that the saliva added on the teeth surface was washed away in a short time by droplets released from instruments after the start of the treatment.

Figure 6 (b), (c), and (d) shows that the mass fraction of droplets with small size (0-20 μm) caused by different injecting flow rates (namely, 40 ml/min, 60 ml/min, and 80 ml/min) of the instrument was 34.4 %, 10.8 %, and 13.1 %, respectively. In general, a lower flow rate of powder-jet-handpieces caused a higher mass fraction of droplets with this range of small size. The possible reason was that a low injecting flow rate of air-powder-polishing would mix sufficiently the released gas and liquid, which should then produce a higher mass fraction of droplets with small size.

Figure 6 (b), (e), (f), and (g) shows that different tooth positions did not have an obvious influence on the droplets size distribution. This may be because that the atomization process at different tooth position was basically the same.

Various combinations of the parameters mentioned above widely occur during the real-life dental treatments, mainly due to the different health conditions of patient's mouth and the different treatment behaviors of the dental workers. It is therefore impossible to obtain a general size distribution of the droplets emitted from the dental treatments. In order to provide a representative size distribution of the emitted droplets, so as to have a better understanding of the emission process and to formulate an initial condition for CFD simulations, the average size distribution of the droplets of the seven different cases was calculated, as listed in Table 4. The Rosin-Rammler particle size distribution is frequently used to indicate the droplets size distribution of liquid sprays [34], which can be defined by the following equation:

$$Y_d = e^{-(d/\bar{d})^n} \tag{1}$$

where Y_d is the mass fraction of droplets with size larger than d; $\bar{d}$ is the mean size of droplets; and n is the size distribution parameter. Figure 7 shows the fitted average experimental data from Table 4 and Table 7 based on the Rosin-Rammler equation, in which the $\bar{d}$ is 54.96 μm (Figure 7 (a)) and 98.93 μm (Figure 7 (b)), and the n is 1.35 and 1.58, respectively.

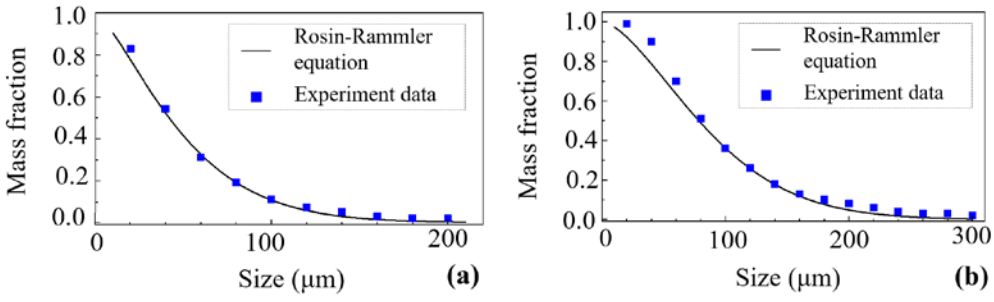

Figure 7 The fitting between the Rosin-Rammler equation and the average size of droplets for Cases 1-7: (a) the process of air-powder-polishing and (b) the process of ultrasonic scaling.

Table 4 Mass fraction distribution of droplets during the process of air-powder-polishing.

Droplets size range (μm)	Case 1 (%)	Case 2 (%)	Case 3 (%)	Case 4 (%)	Case 5 (%)	Case 6 (%)	Case 7 (%)	Mean (%)
2-20	11.1	10.8	34.4	13.1	15.1	15.0	18.3	16.8
20-40	24.5	27.4	39.0	29.4	24.2	29.7	30.5	29.2
40-60	23.0	24.8	15.4	20.6	24.5	25.5	24.1	22.6
60-80	15.0	14.9	5.9	11.9	14.6	13.6	13.0	12.7
80-100	10.0	9.2	2.9	8.0	8.6	7.4	7.3	7.6
100-120	5.6	4.8	1.2	5.0	4.1	3.3	3.3	3.9
120-140	3.7	3.0	0.7	3.7	2.4	1.9	1.8	2.5
140-160	2.4	1.9	0.3	2.7	1.5	1.2	0.9	1.6
160-180	1.4	1.1	0.1	1.8	0.9	0.7	0.4	0.9
180-200	1.0	0.8	0.1	1.3	0.8	0.5	0.2	0.7
200-220	0.8	0.6	0.1	1.0	0.7	0.4	0.1	0.5
220-240	0.5	0.4	0.0	0.6	0.6	0.3	0.0	0.3
240-260	0.4	0.3	0.0	0.4	0.5	0.2	0.0	0.3
260-280	0.2	0.1	0.0	0.2	0.4	0.1	0.0	0.2
280-300	0.2	0.1	0.0	0.1	0.4	0.1	0.0	0.1
300-320	0.1	0.0	0.0	0.0	0.3	0.0	0.0	0.1
320-340	0.1	0.0	0.0	0.0	0.3	0.0	0.0	0.1
>340	0.0	0.0	0.0	0.0	0.3	0.0	0.0	0.0
Summary	100.0	100.0	100.0	100.0	100.0	100.0	100.0	100.0

3.2 Flow-field characteristics

3.2.1 Time averaged velocities

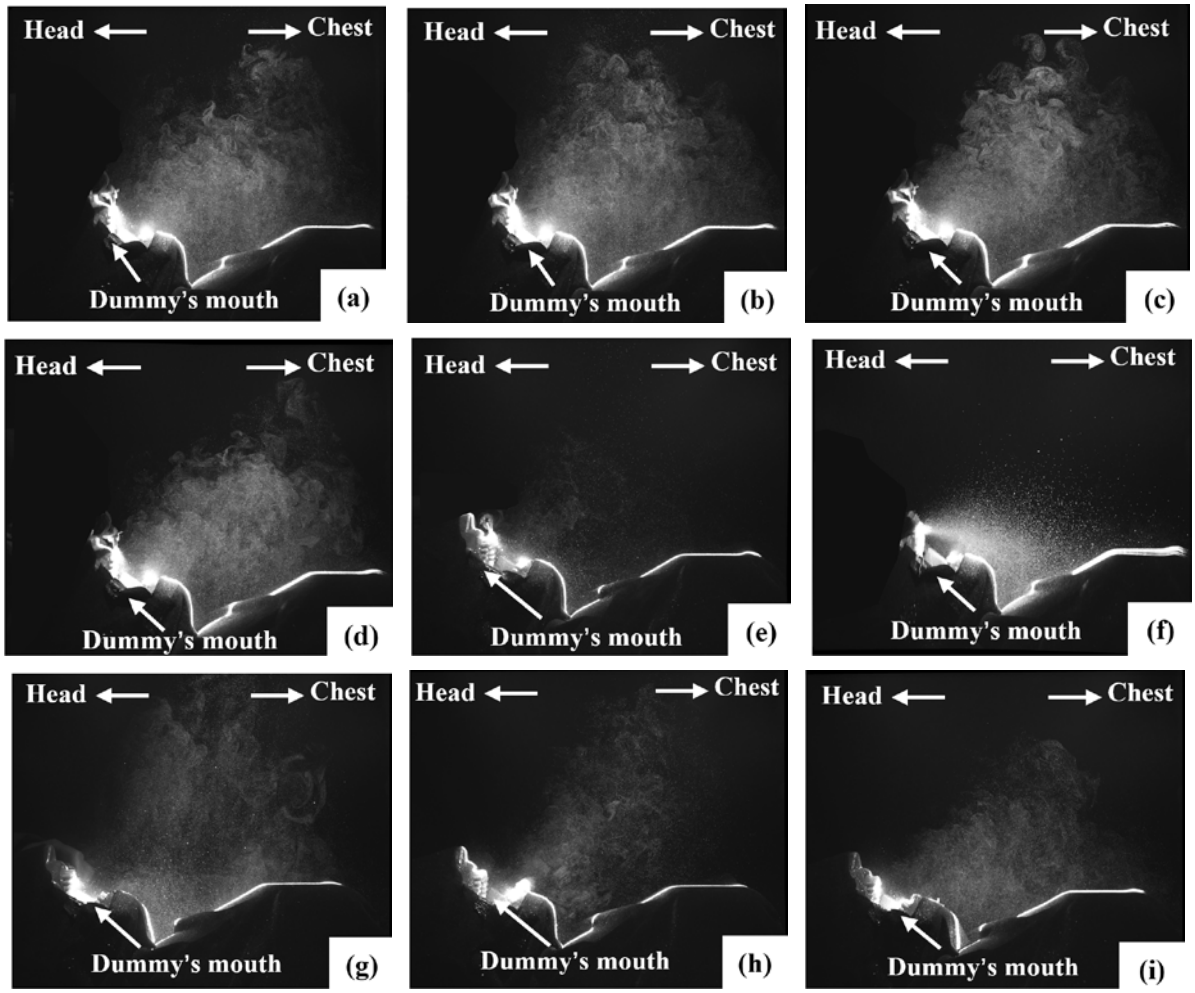

Figure 8 Droplets distribution on the measured planes during the process of air-powder-polishing: (a) Case 1, (b) Case 2 P0, (c) Case 2 P1, (d) Case 2 P2, (e) Case 3, (f) Case 4, (g) Case 5, (h) Case 6, and (i) Case 7. Note: Each photo was formed from multiple instantaneous photo overlays.

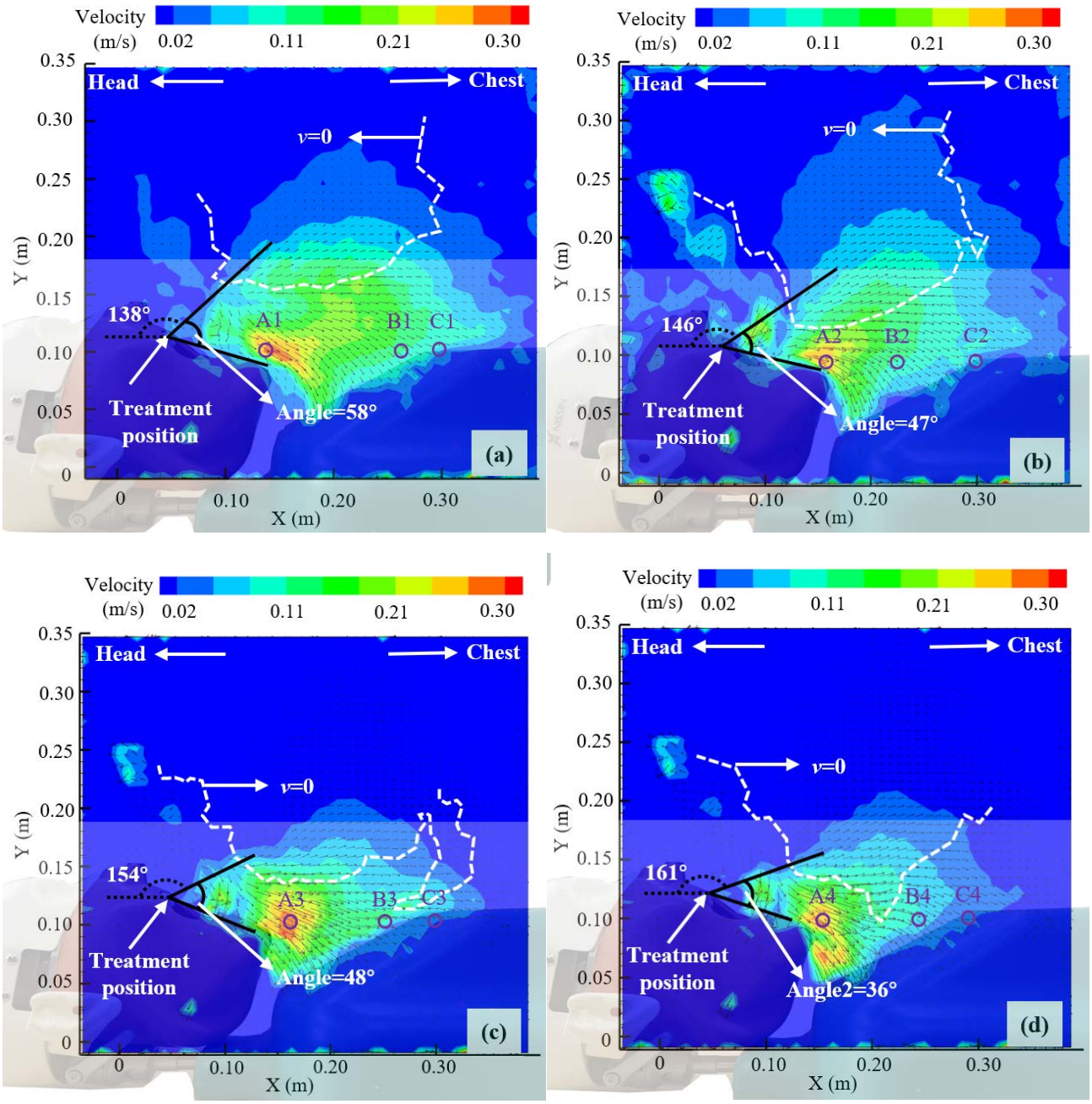
Velocity
(m/s) 0.02 0.11 0.21 0.30
Head
Chest
v=0
138°
A1
B1
C1
Treatment position
Angle=58°
(a)
146°
A2
B2
C2
Angle=47°
(b)
154°
A3
B3
C3
Angle=48°
(c)
161°
A4
B4
C4
Angle2=36°
(d)
Y (m)
X (m)
0
0.05
0.10
0.15
0.20
0.25
0.30
0.35

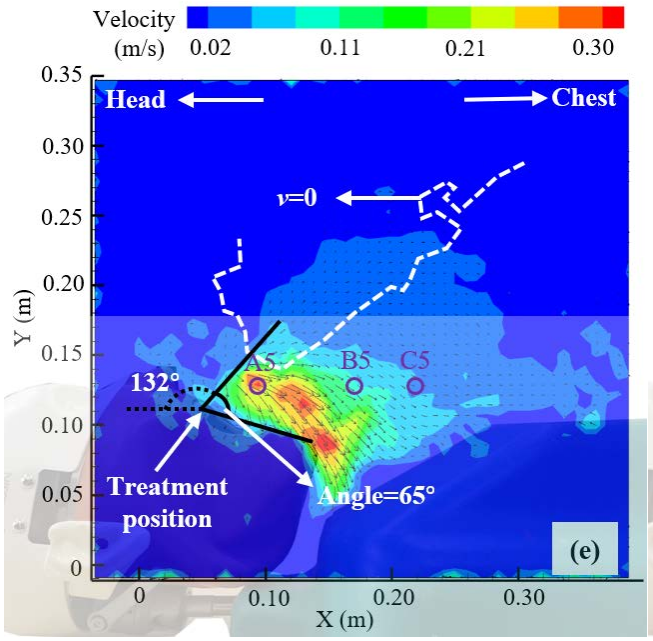
Velocity
(m/s) 0.02 0.11 0.21 0.30
Head
Chest
v=0
A5
B5
C5
132°
Treatment position
Angle=65°
(e)
Y (m)
X (m)

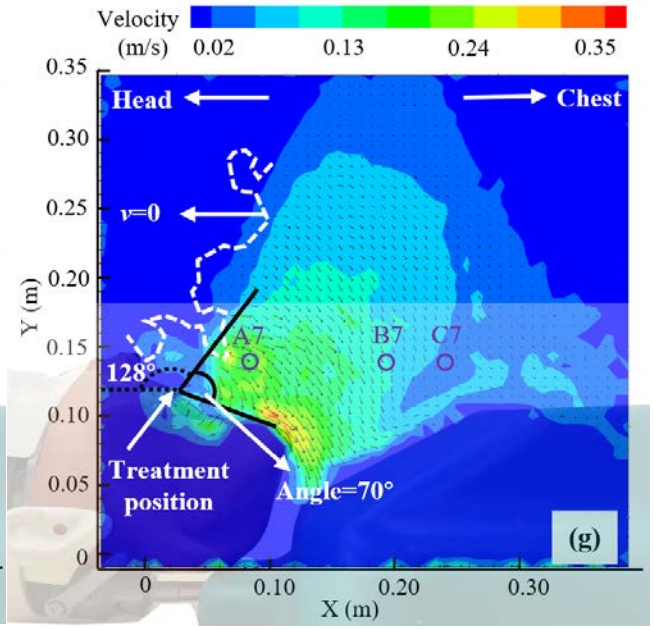
Velocity
(m/s) 0.02 0.13 0.24 0.35
Head
Chest
v=0
A7
B7
C7
128°
Treatment position
Angle=70°
(g)
Y (m)
X (m)

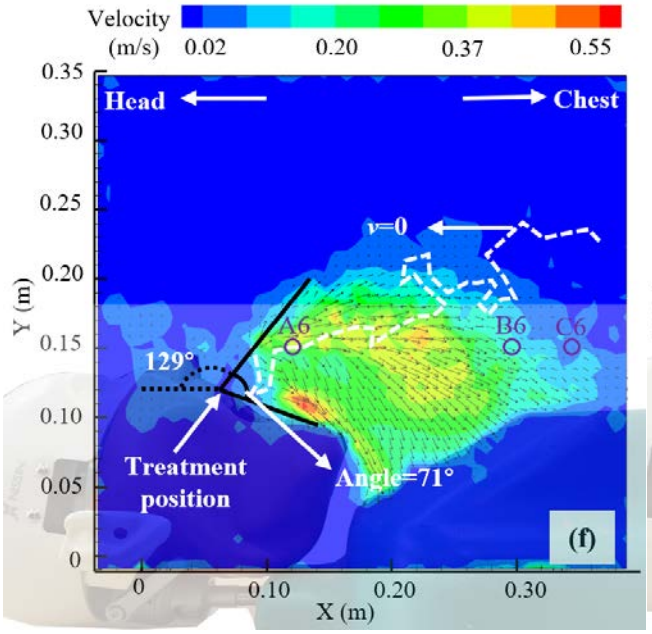
Velocity
(m/s) 0.02 0.20 0.37 0.55
Head
Chest
v=0
A6
B6
C6
129°
Treatment position
Angle=71°
(f)
Y (m)
X (m)

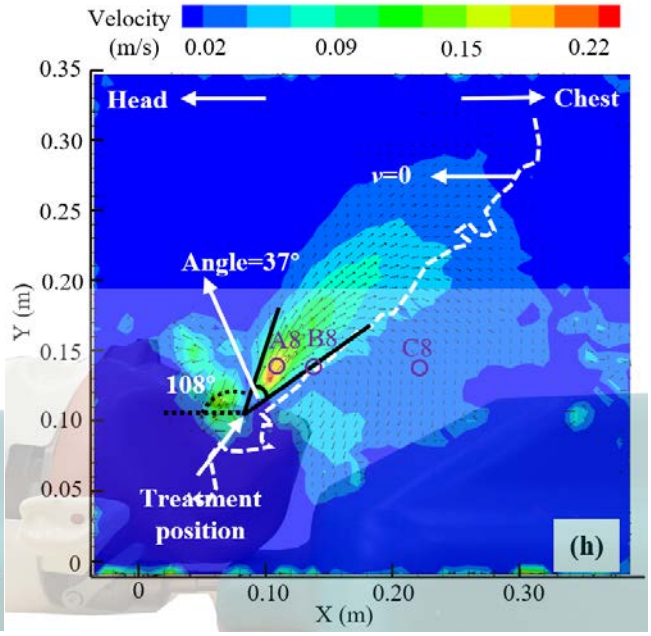
Velocity
(m/s) 0.02 0.09 0.15 0.22
Head
Chest
v=0
Angle=37°
A8
B8
C8
108°
Treatment position
(h)
Y (m)
X (m)

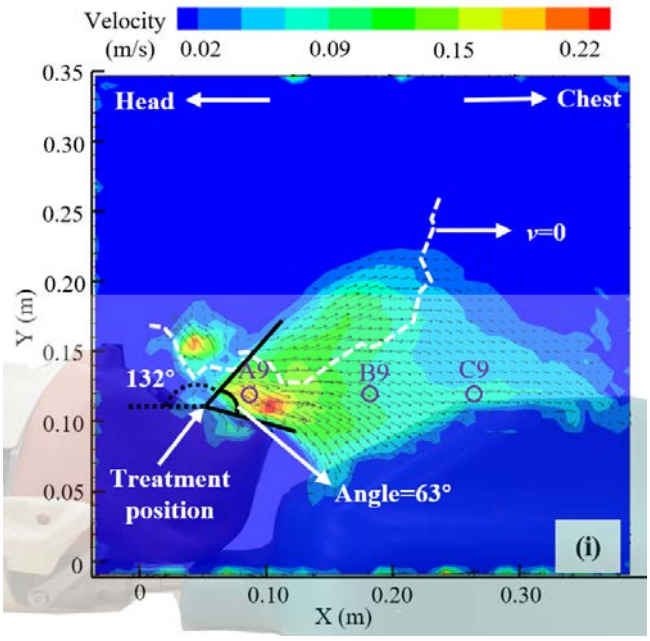

Figure 9 Time averaged distribution of synthetized velocity of droplets generated by using the powder-jet-handpieces (based on 200 samples): (a) Case 1 (60 ml/min; 9th tooth), (b) Case 2 P0 (60 ml/min; 9th tooth), (c) Case 2 P1 (60 ml/min; 9th tooth), (d) Case 2 P2 (60 ml/min; 9th tooth), (e) Case 3 (40 ml/min; 9th tooth), (f) Case 4 (80 ml/min; 9th tooth), (g) Case 5 (60 ml/min; 12th tooth), (h) Case 6 (60 ml/min; 24th tooth), and (i) Case 7 (60 ml/min; 21st tooth)

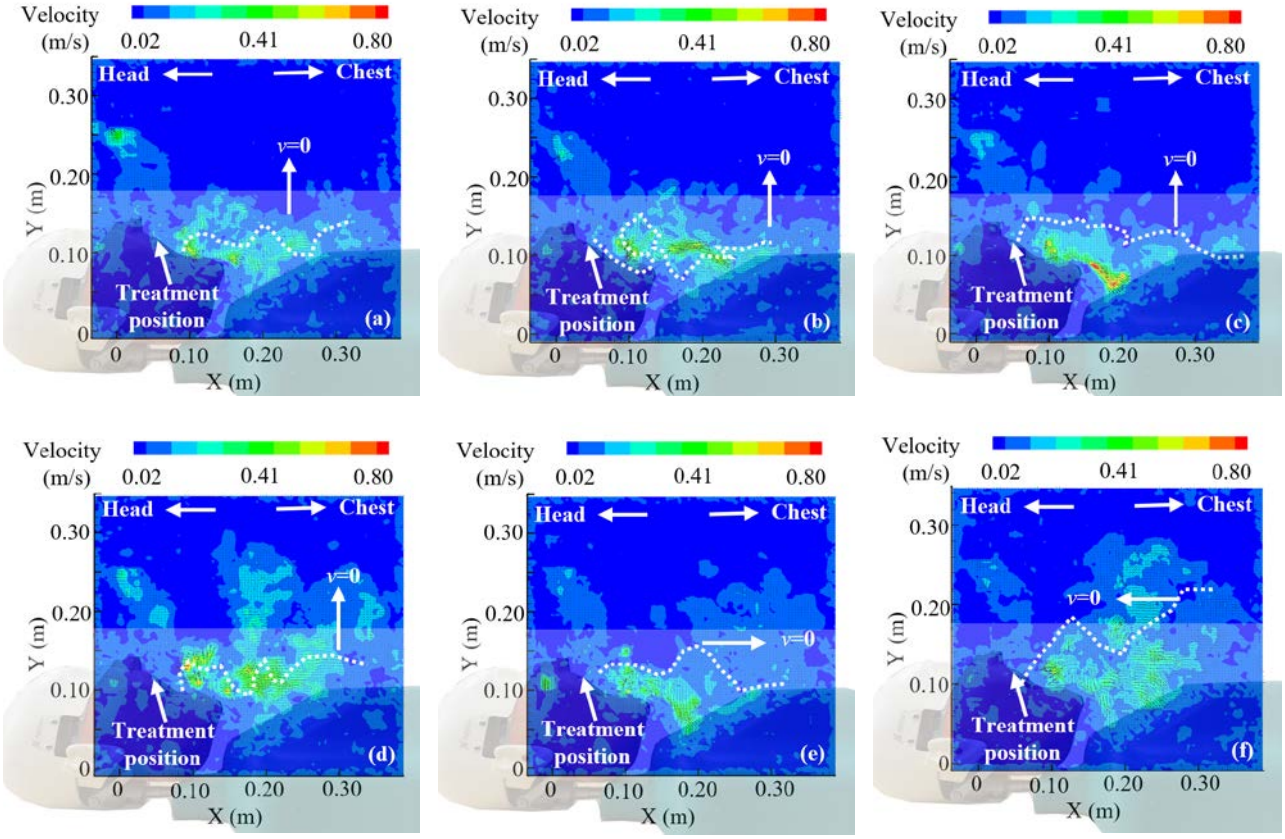

Figure 10 Instantaneous synthetized velocity distribution of droplets generated by using the powder-jet-handpieces: (a) 0.25 s (Case 1), (b) 0.5 s (Case 1), (c) 1.0 s (Case 1), (d) 0.25 s (Case 2 P0), (e) 0.5 s (Case 2 P0), and (f) 1.0 s (Case 2 P0).

To clearly show the distribution of the droplets cloud around the dummy's mouth, the multiple instantaneous photos were overlaid, as shown in Figure 8. The cases in Figure 8 correspond to those in Figure 9. Each plot in Figure 9 was the average distribution during the measurement within 40 s (totally 200 samples). In Figure 9 and later-on figures, the velocities were synthetized by *u*, velocity along X-axis, and *v*, velocity along Y-axis. To distinguish the rising and falling areas of droplets, a line of *v*=0 was plotted in Figure 9. The droplets in Figure 8 and Figure 9 were the combinations of three parts, namely the droplets bounced back into the air after impacting the teeth, those escaped from the mouth and into the air due to the wall effect, and those moved into the air. Meanwhile, there were moving airflows around the mouth, which also affected the distribution of the droplets. These factors complicated the flow field and emission characteristics near the dummy's mouth during the process of air-powder-polishing.

Emission angle of droplets generated during the process of the air-powder-polishing is also an important emission characteristic and initial boundary condition for CFD simulations. In Figure 9, the emission direction of a few droplets was towards the top of the dummy's head. Major portion of droplets moved towards the dummy's chest and the region above the chest, which was, therefore, the dominant emission direction. The emitted droplets formed approximately a cone shape, and its angle varied from 37°

(Figure 9 (h)) to 71° (Figure 9 (f)). In addition, the velocity distribution of droplets under different cases was very similar, less than 0.35 m/s.

The emission angles of droplets under the conditions without and with artificial saliva were 58° and 47°, as shown in Figure 9 (a) and (b). In general, the condition without applying artificial saliva presented a slightly larger emission range of air speed greater than 0.1 m/s, with the boundary of v=0 at a higher position. However, it must be noted that the artificial saliva was applied on teeth before the experiments and there was no continuous addition. Considering that the time of air-powder-polishing was relatively long (40 s) and the artificial saliva would be quickly washed by droplets released from the powder-jet-handpieces, there should be only a little influence of saliva on the time averaged distribution of droplets. Therefore, it is necessary to analyze the instantaneous distributions of droplets related to Figure 9 (a) and (b) at the beginning of air-powder-polishing, which are shown in Figure 10. Overall, the condition without applying artificial saliva presented a slightly smaller emission range, including those range above the line of v=0. The difference between the time averaged and instantaneous distribution can also be explained by that the presence of saliva increases the percentage of larger droplets that have higher momentums to move farther from the treatment sites. The maximum velocity of droplets for the two conditions was quite close. It may be reasonable to expect that the real-life condition with continuous secretion of saliva would come with more large droplets and thus an even larger emission range.

Figure 9 (b), (c), and (d) show the time averaged distribution of synthetized velocity at different measured planes. In general, the emission range decreased with the increase of distance away from the treatment site, which was indicated by both the area of the droplets and the emission angle. At the plane across the treatment site, there was a larger portion of droplets moving towards ceiling, implying the high risk of dental workers with the head above the dummy's head. Despite of a smaller range, the appearance of the droplets at the planes away from the treatment site, with comparable speed, meant the extension of the droplet distribution towards the horizontal direction, which might support the existing knowledge that the droplets released into the air from the treatment site formed a cone shape. However, limited by the experimental technology and resources, it was difficult to figure out the boundary of the droplet distribution in the horizontal direction. In the following sections, only the vertical plane at the treatment site was selected for analysis.

The flow rates of powder-jet-handpieces corresponding to Figure 9 (b), (e), and (f) were 60 ml/min, 40 ml/min, and 80 ml/min. With the flow rate increased, the emission range with greater velocities was larger. The reason should be that a greater flow rate holds a higher emission momentum. The emission angles corresponding to smaller and larger flow rates were larger than that with the middle flow rate, implying that there was no linear relation between the emission angle and flow rate. The possible reason is that the teeth surfaces are not flat planes but irregular surfaces. After droplets impacting the teeth, the emission angles have uncertainty and so do not necessarily increase or decrease with the flow rate. Overall, the velocities were larger at the flow rate of 80 ml/min than those at 40 or 60 ml/min. In fact, the flow rates commonly used by medical

workers are 40-60 ml/min, meaning low emission velocities and ranges in practice. These results suggest the selection of lower flow rates if possible.

Figure 9 (b), (g), (h), and (i) correspond to the treatment on the tooth No 9, 12, 24, and 21, respectively. The emission ranges at the 9th, 12th, and 21st teeth were similar, which were larger than that at the 24th tooth. Compared with side teeth, the front teeth have flatter plane. However, the emission angles at the front teeth were smaller than that at the side teeth, namely, 47° (Figure 9 (b), 9th tooth) < 70° (Figure 9 (g), 12th tooth) and 37° (Figure 9 (h), 24th tooth) <63° (Figure 9 (i), 21st tooth), implying that the teeth planeness may be the main factor influencing emission angle. In terms of maximum velocities in each plot, compared with mandibular teeth, the maxillary teeth have larger velocities, namely, 0.3 m/s (Figure 9 (b), 9th tooth) > 0.22 m/s (Figure 9 (h), 24th tooth) and 0.35 m/s (Figure 9 (g), 12th tooth) > 0.22 m/s (Figure 9 (i), 21st tooth). Note that the emission direction at the 9th and 12th maxillary tooth was towards the dummy's upper region and the chest, while, except for the two directions, the emission direction at the 24th and 21st mandibular tooth was towards the dummy's head direction, moving at the velocity of 0.15 m/s (Figure 9 (h)) and 0.22 m/s (Figure 9 (i)). This indicated that scattered emission directions appeared when mandibular teeth were treated. Control measures should take into account such emission characteristics.

3.2.2 Time averaged vorticity

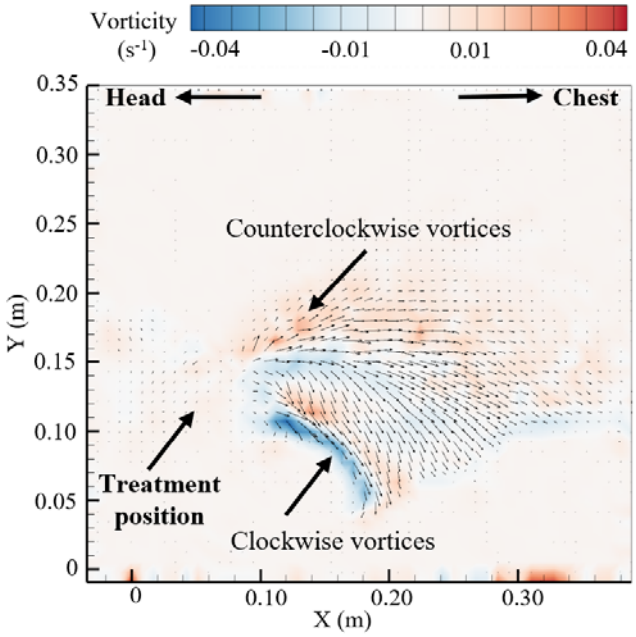

Figure 11 The time averaged vorticity distribution of droplets during the use of the powder-jet-handpieces: Case 4 (80 ml/min; 9th tooth).

Vorticity reflects the strength and direction of vortices. The time averaged vorticity analysis is necessary, because vortices around the dummy's mouth may cause droplets accumulation around the respiratory zone of dental workers, increasing their exposure risk. The vorticity was expressed by the following equation:

$$Vorticity = \frac{dV}{dx} - \frac{dU}{dy} \quad (2)$$

Different cases have similar vorticity sizes and distribution characteristics, and thus the Case 4 was selected for analysis. As shown in Figure 11, the vortices around the dummy's mouth included positive vortices (counter clockwise vortices) and negative vortices (clockwise vortices). The negative vortices appeared at the lower part of the emission region, while the positive vortices appeared at the upper part of the emission region. The appearance of the positive vortices may be related to the buoyancy effect of droplets with small sizes and the influence of gas released by the powder-jet-handpieces. Positive vortices may drive droplets with small size and low velocity to suspend at the height of the respiratory zone of medical workers, increasing the exposure risk. The reason for the negative vortices is that droplets with large sizes settled to the surfaces along the direction of the dummy's chest due to the gravitational influence, resulting in probable severe surface contamination. In Figure 11, the minimum vorticity of all cases was -0.04 s^{-1} and the maximum was 0.04 s^{-1}, indicating that the vortices strength is small near the dummy's mouth. However, considering the long-term exposure of medical workers in such an environment during working period, methods for vortices removal should still be necessary.

3.2.3 Velocity variation at typical locations

The above analysis showed that there was a varying range of the droplets generated by using the powder-jet-handpieces under different conditions. The droplets with large size settled to the surfaces rapidly within a short distance due to the gravitational influence. The droplets with small size were rapidly dehydrated, and they were less affected by gravity and can suspend in the air for a long time. These may cause airborne transmission of infectious diseases, increasing the exposure risk of medical workers and the patients who visited later.

In Figure 9, three locations were representative. Location A represented the position with the largest velocity near the dummy's mouth. Location C was at the edge of emission area at the same height with Location A. Location B was between A and C, and the velocities at the left and right regions of Location B had an obvious difference. It is interesting to analyze the velocity fluctuation over time at these three locations during the measurement. The velocity coordinates and distribution of these three points were presented in Table 5 and Figure 12, respectively.

Table 5 Coordinates of key locations in the measured plane during the process of air-powder-polishing.

Points	Case 1	Case 2 P0	Case 2 P1	Case 2 P2	Case 3	Case 4	Case 5	Case 6	Case 7
A	(0.14,0.10)	(0.16,0.10)	(0.16,0.10)	(0.15,0.10)	(0.09,0.13)	(0.12,0.15)	(0.08,0.14)	(0.10,0.14)	(0.08,0.12)
B	(0.26,0.10)	(0.22,0.10)	(0.25,0.10)	(0.24,0.10)	(0.17,0.13)	(0.30,0.15)	(0.19,0.14)	(0.14,0.14)	(0.18,0.12)
C	(0.29,0.10)	(0.30,0.10)	(0.30,0.10)	(0.29,0.10)	(0.22,0.13)	(0.34,0.15)	(0.24,0.14)	(0.22,0.14)	(0.26,0.12)

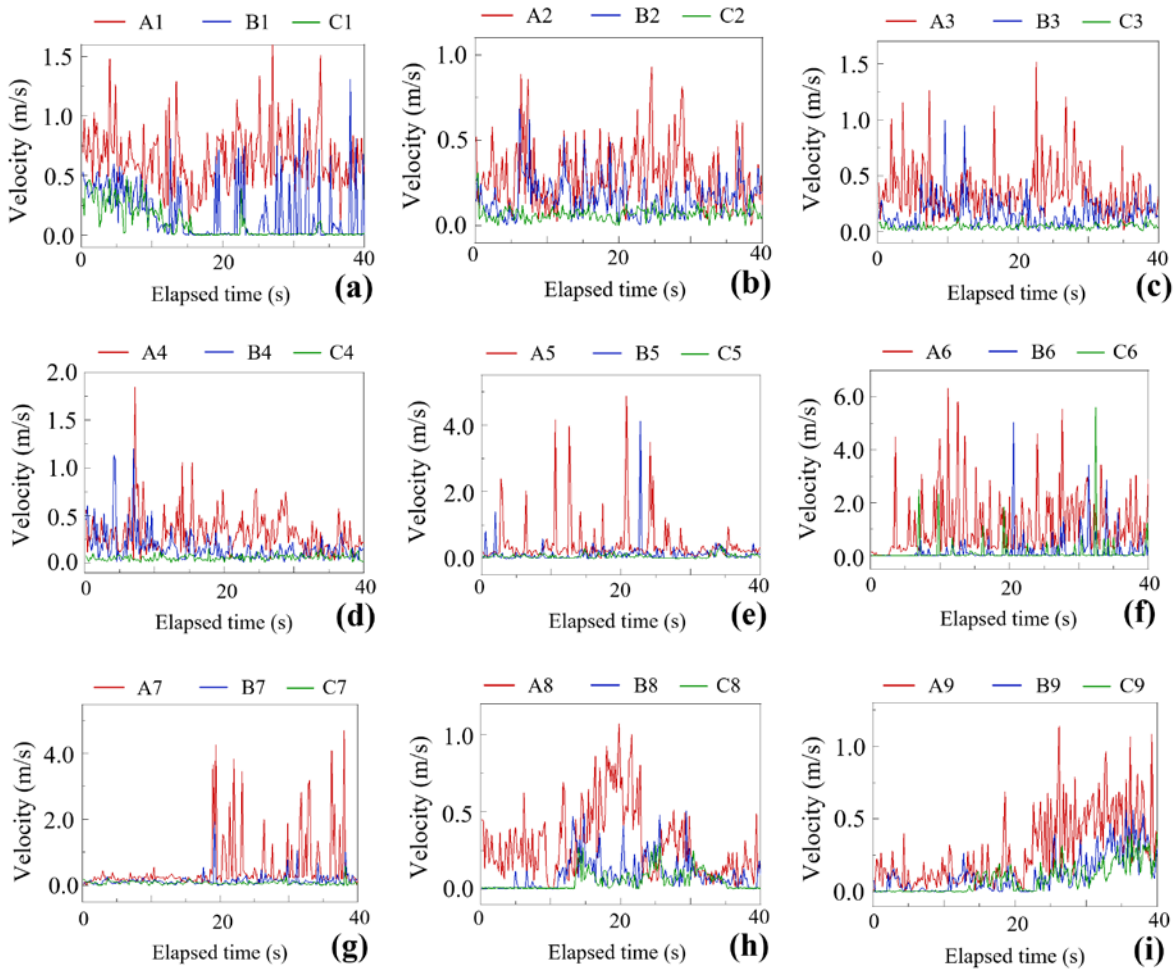

Figure 12 Instantaneous synthetized velocity distribution of droplets generated by using the powder-jet-handpieces at three typical locations:(a) Case 1, (b) Case 2 P0, (c) Case 2 P1, (d) Case 2 P2, (e) Case 3, (f) Case 4, (g) Case 5, (h) Case 6, and (i) Case 7.

In Figure 12, the maximum velocity at the location A in all cases were close to or exceeds 1.0 m/s, and the maximum value appeared in Figure 12 (f), reaching about 6.0 m/s. The synthesis velocities at the locations B and C also approached to or exceed 1.0 m/s at a few times in some cases, such as in Figure 12 (e) and (f). In general, velocity at the location A fluctuated most, followed by the locations B and C, and their order of magnitude of the standard deviation came to be 10^{-1},10^{-2}, and 10^{-2}, respectively. The reason for the fluctuation is basically the turbulent nature of the flow and particle dynamics. In the present, the measured period of each case was 40 s, which is much longer than the 5 s used in existing studies [26].

3.2.4 Maximum velocities closed to dummy's mouth

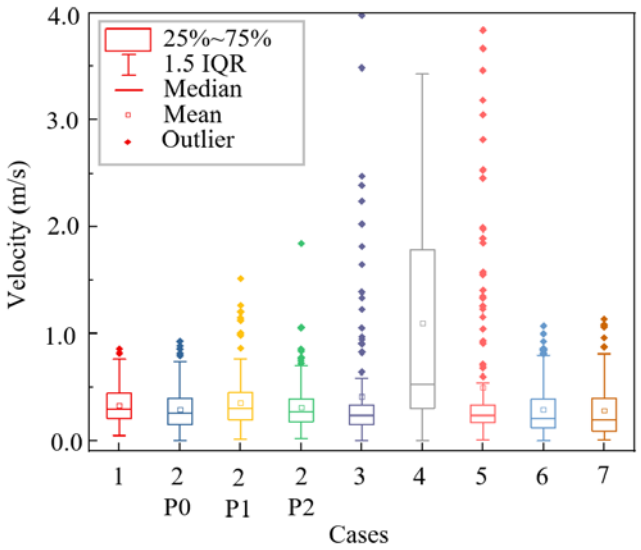

Figure 13 Synthetic velocity distribution of the location (A) with the highest velocity under different conditions during the process of air-powder-polishing.

In CFD simulation, the mouth as a point source to release droplets in a cone shape, approximately representing the pollution generation process. In addition to the cone angle, the initial velocity at the point source, namely the mouth, was also an important boundary condition. The box plot of the velocity of point A of each case (40 s) was presented in Figure 13, and some key values were listed in Table 6.

Table 6 Key values in synthetic velocity distribution of droplets during the process of air-powder-polishing.

Key values	Case 1	Case 2 P0	Case 2 P1	Case 2 P2	Case 3	Case 4	Case 5	Case 6	Case 7
Minimum	0.01	0.00	0.02	0.02	0.00	0.00	0.01	0.00	0.01
Maximum	0.76	0.74	0.76	0.70	0.59	3.42	0.54	0.80	0.81
Mean	0.30	0.26	0.30	0.27	0.24	0.53	0.23	0.21	0.19
Median	0.33	0.28	0.35	0.31	0.42	1.11	0.51	0.29	0.28

4 Discussions

In this study, the size distribution and flow-field characteristics of droplets generated during the use of powder-jet-handpieces and ultrasonic scaling instrument were quantified and visualized. These findings increase the understanding of the characteristics of droplets generated during dental treatments. These findings provide important boundary conditions for CFD simulation, which would be helpful to assess the exposure risk of people around and to develop new control measures.

The size and velocity of the emitted droplets are key parameters characterizing the droplet emission. Previous studies on the characteristics of droplet emission during dental treatments focused mainly on the teeth cleaning with the use of ultrasonic scaling instruments. A variety of measurement techniques have been used, including PIV and image particle counter [26], optical flow tracking velocimetry [27], digital inline

holography and laser sheet imaging method [29], and tracer particle and impacting method [30]. Since the tracer particle and impacting method cannot efficiently consider the evaporation of droplets [29], which may not be as accurate as the image based methods. However, the image based methods generated only two dimensional results. The limitation of the above studies based on image measurement method is that they are two dimensional results, which is also the limitation of the current technology. Regardless of this, our study on the emission characteristics of droplets can further help to characterize the movement and transport of droplets in the clinic.

Emission angle is another important parameter characterizing droplet emission. An emission shape with a cone, and an emission angle of 30° were widely used in past CFD simulations as boundary conditions [35-37]. The findings of the present study showed that such a parameter could change largely with the difference in tooth flatness, tooth position, and flow rate. Specifically, it was shown that, at the maxillary teeth position, the emission angle at the 9^{th} tooth was 20° larger than that at the 12^{th} tooth, and the obvious difference also appeared at the mandibular teeth (namely, the 24^{th} and 21^{st} tooth). In addition, the flow rate largely affected the initial velocity and emission angle. Increasing the flow rate from 60 ml/min to 80 ml/min led to the increase of the initial velocity by 0.2 m/s and the emission angle by 25°. The influence of these differences in the initial boundary condition of droplet emission on the distribution of droplets indoors, the fate of the emitted droplets, and the exposure risk of people around are still awaiting for explorations.

5 Conclusions

This study examined the size distribution and flow-field emission characteristics of droplets generated during the use of powder-jet-handpieces and ultrasonic scaling instrument. The following conclusions may be drawn.

The peak mass fraction of droplets during the air-powder-polishing and ultrasonic scaling processes occurs around the droplet size from 20 μm to 40 μm, while, for all cases, the mass fraction of droplets with the diameter less than 100 μm accounts for over 80%. The tooth position has a negligible influence on the droplet size distribution, but the injecting flow rate largely determines the mass fraction of droplets with small size (0-20 μm), which are 34.4 %, 10.8 %, and 13.1 % for 40 ml/min, 60 ml/min, and 80 ml/min, respectively. By fitting the mass fraction distribution of droplets emitted during the use of air-powder-polishing with the Rosin-Rammler equation, the mean size of droplets ($\bar{d}$) and the size distribution parameter (n) are 54.96 and 1.35, respectively.

Major portion of droplets moved towards the dummy's chest and the region above the chest, which is the dominant emission direction. The emitted droplets formed approximately a cone shape, and its angle varied from 37° to 71° for different conditions. In addition, the mean velocity of droplets under different cases was similar, mostly less than 0.35 m/s.

The injecting flow rate and treated tooth position are the major factors influencing the emission direction, angle, and velocity. The influence of injecting flow rate is not linear, as the teeth surfaces are not flat planes but the irregular surfaces. The emission angles at the front teeth were smaller than that at the side teeth, implying that the teeth

planeness is an important factor influencing emission angle. Scattered emission directions appeared when mandibular teeth are treated, while the treatment on maxillary teeth give larger emission velocities.

The maximum velocity of droplets at the location near the dummy's mouth is close or exceeds 1.0 m/s for most conditions. The velocity fluctuates strongly at such locations, with the standard deviation at the order of magnitude of 10^{-1}, which is 10^{-2} at other locations at the same height.

The findings of this study increase our understanding of the emission characteristics during dental treatments and improve the accuracy of boundary conditions for CFD simulations, which would be helpful for the development of the new control measures.

Acknowledgement

This study was supported by the Fundamental Research Funds for the Central Universities (No. 531118010378). The authors would like to thank chenzhi Cai and hanfeng Wang for providing PIV platform.

Appendix

See Figure 14, Figure 15, Figure 16, Figure 17, Figure 18, Figure 19, Table 7, Table 8, and Table 9.

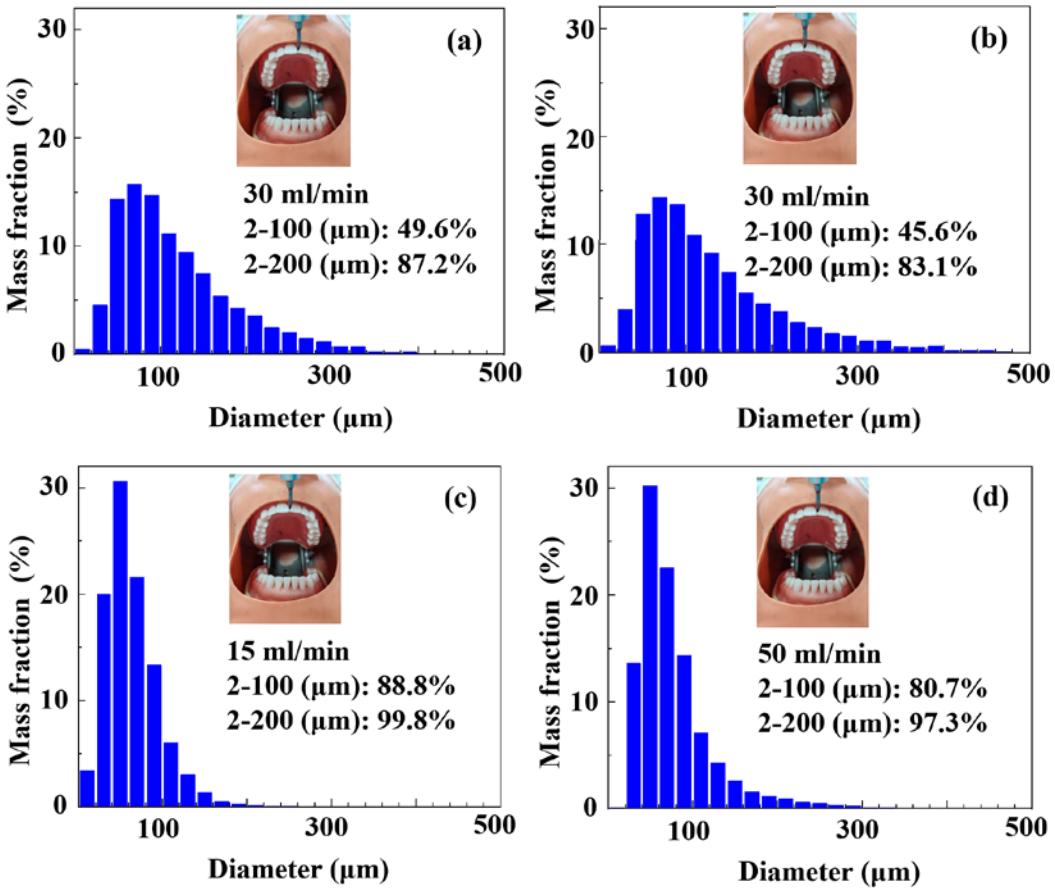

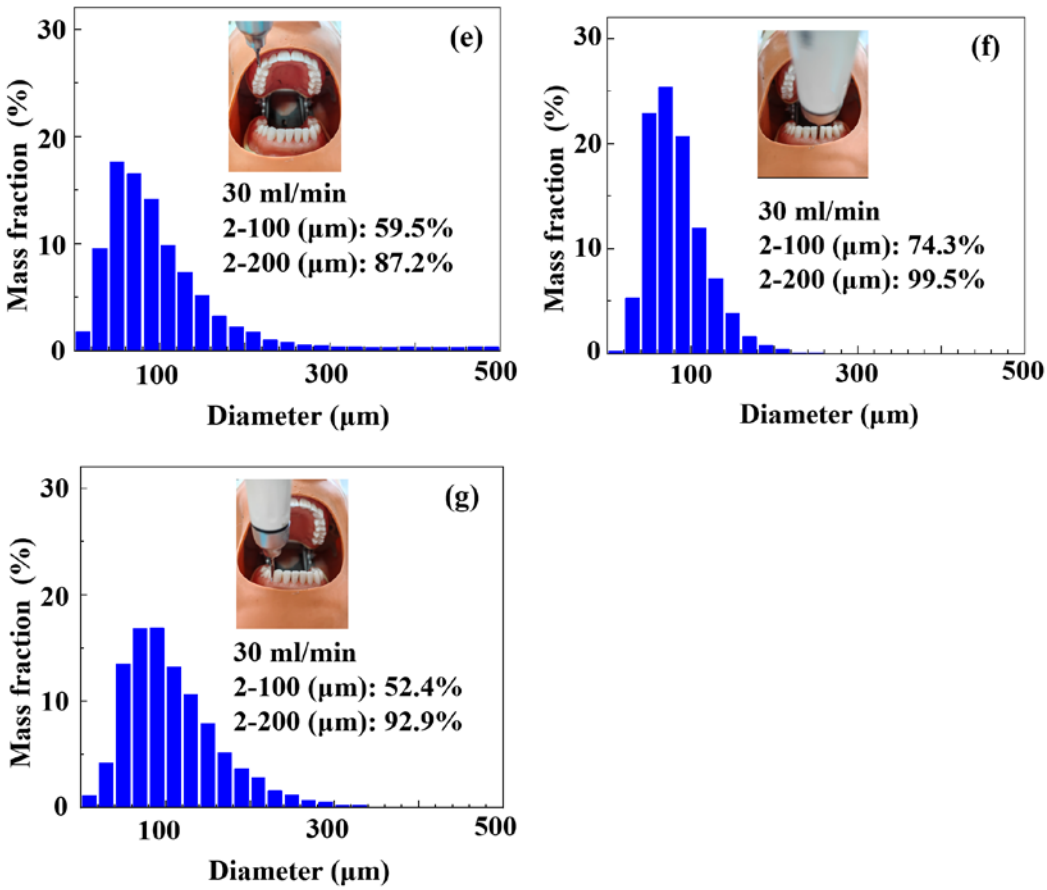

Figure 14 The mass fraction distribution of droplets size during the process of ultrasonic scaling: (a)-(g) corresponding to Cases 1-7.

Table 7 Mass fraction distribution of droplets during the process of ultrasonic scaling.

Droplets size range (μm)	Case 1 (%)	Case 2 (%)	Case 3 (%)	Case 4 (%)	Case 5 (%)	Case 6 (%)	Case 7 (%)	Mean (%)
2-20	0.4	0.7	3.4	0.1	1.7	0.2	1.1	1.1
20-40	4.5	4.0	20.0	13.6	9.5	5.3	4.2	8.7
40-60	14.3	12.9	30.5	30.2	17.6	22.9	13.5	20.3
60-80	15.7	14.4	21.6	22.5	16.5	25.4	16.8	19.0
80-100	14.7	13.8	13.3	14.3	14.1	20.7	16.9	15.4
100-120	11.1	10.9	6.0	7.1	9.8	11.9	13.2	10.0
120-140	9.4	9.2	3.0	4.3	7.3	7.1	10.6	7.3
140-160	7.4	7.4	1.4	2.6	5.2	3.8	7.9	5.1
160-180	5.4	5.5	0.5	1.6	3.2	1.6	5.1	3.3
180-200	4.3	4.5	0.2	1.1	2.3	0.8	3.7	2.4
200-220	3.6	3.8	0.1	0.9	1.7	0.4	2.8	1.9
220-240	2.5	2.8	0.0	0.6	1.0	0.1	1.6	1.2
240-260	2.0	2.3	0.0	0.5	0.8	0.0	1.2	1.0
260-280	1.4	1.8	0.0	0.3	0.5	0.0	0.7	0.7
280-300	1.2	1.5	0.0	0.2	0.5	0.0	0.5	0.6

300-320	0.7	1.1	0.0	0.1	0.4	0.0	0.2	0.3
320-340	0.7	1.1	0.0	0.1	0.4	0.0	0.2	0.3
340-360	0.2	0.5	0.0	0.0	0.3	0.0	0.0	0.2
360-380	0.2	0.5	0.0	0.0	0.3	0.0	0.0	0.2
380-400	0.2	0.6	0.0	0.0	0.4	0.0	0.0	0.2
>400	0.00	0.7	0.0	0.0	1.6	0.0	0.0	0.3
Summary	99.8	99.7	100.0	100.0	95.0	100.0	100.0	99.2

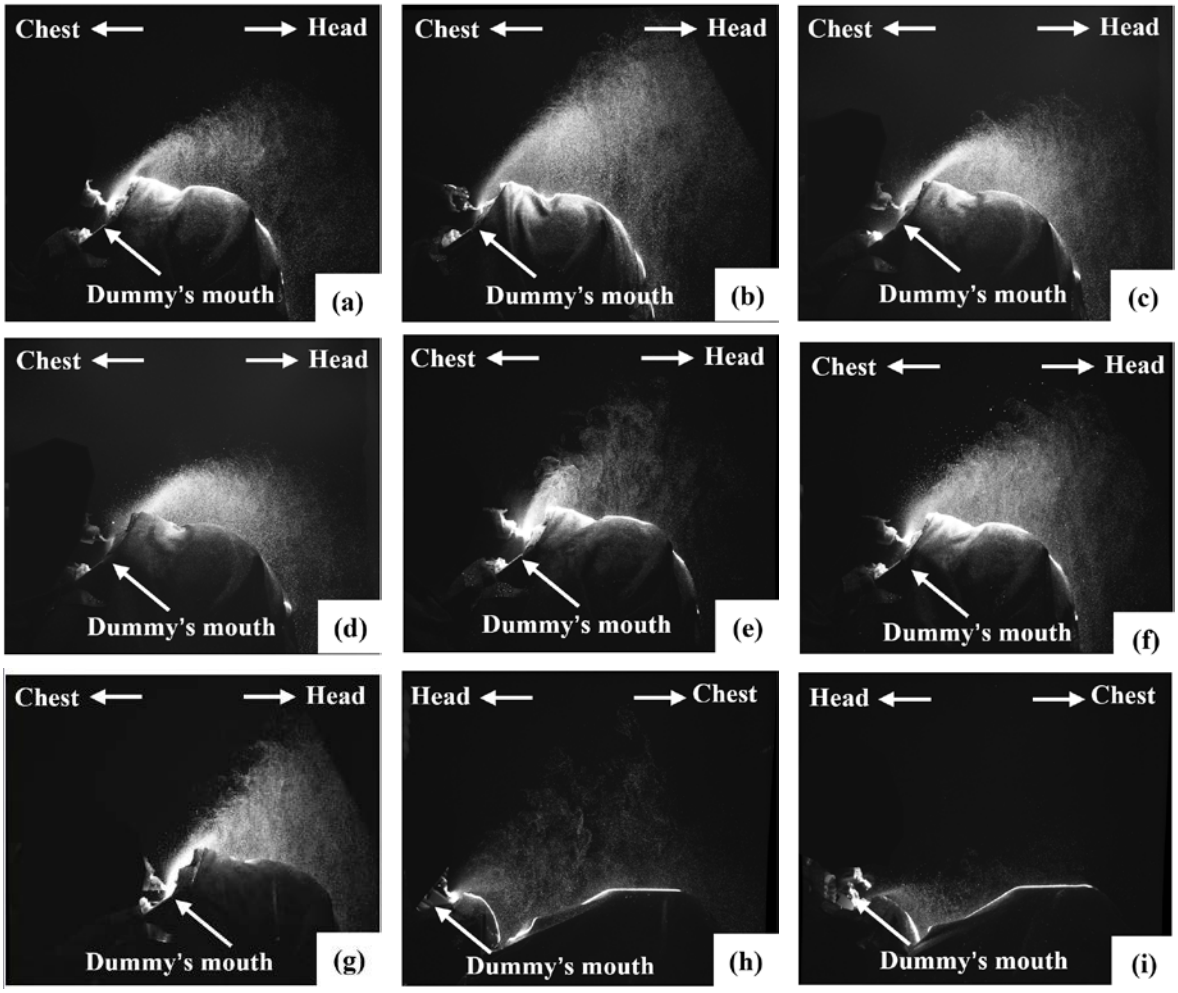

Figure 15 Droplets distribution in measured planes during the process of ultrasonic scaling: (a) Case 1, (b) Case 2 G0, (c) Case 2 G1, (d) Case 2 G2, (e) Case 3, (f) Case 4, (g) Case 5, (h) Case 6, (i) Case 7. Note: Each photo was formed from multiple instantaneous photo overlays.

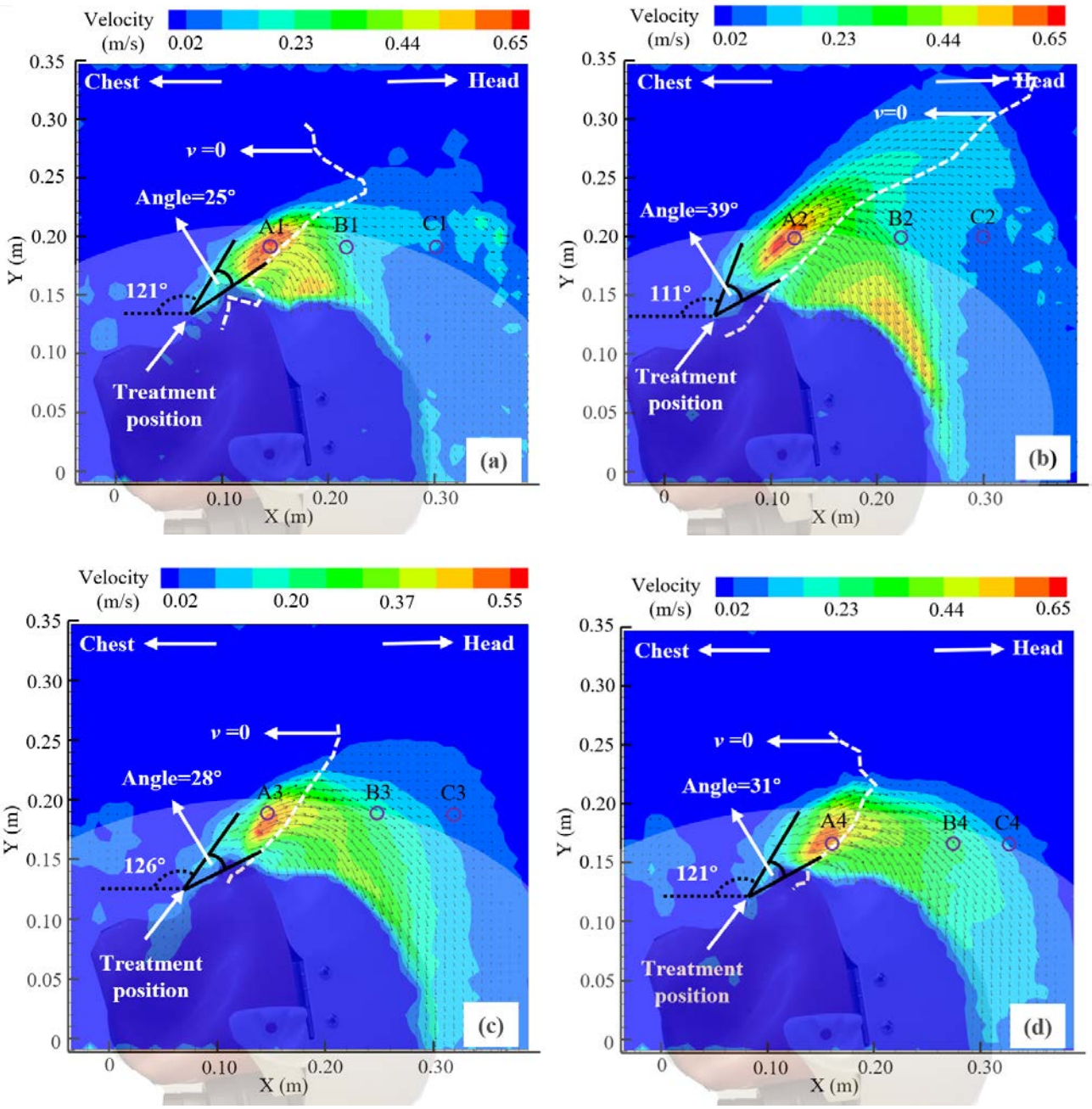
Velocity (m/s) 0.02 0.23 0.44 0.65
Chest
Head
v =0
Angle=25°
A1
B1
C1
121°
Treatment position
(a)
Y (m)
X (m)
Velocity (m/s) 0.02 0.23 0.44 0.65
Chest
Head
v=0
Angle=39°
A2
B2
C2
111°
Treatment position
(b)
Y (m)
X (m)
Velocity (m/s) 0.02 0.20 0.37 0.55
Chest
Head
v =0
Angle=28°
A3
B3
C3
126°
Treatment position
(c)
Y (m)
X (m)
Velocity (m/s) 0.02 0.23 0.44 0.65
Chest
Head
v =0
Angle=31°
A4
B4
C4
121°
Treatment position
(d)
Y (m)
X (m)

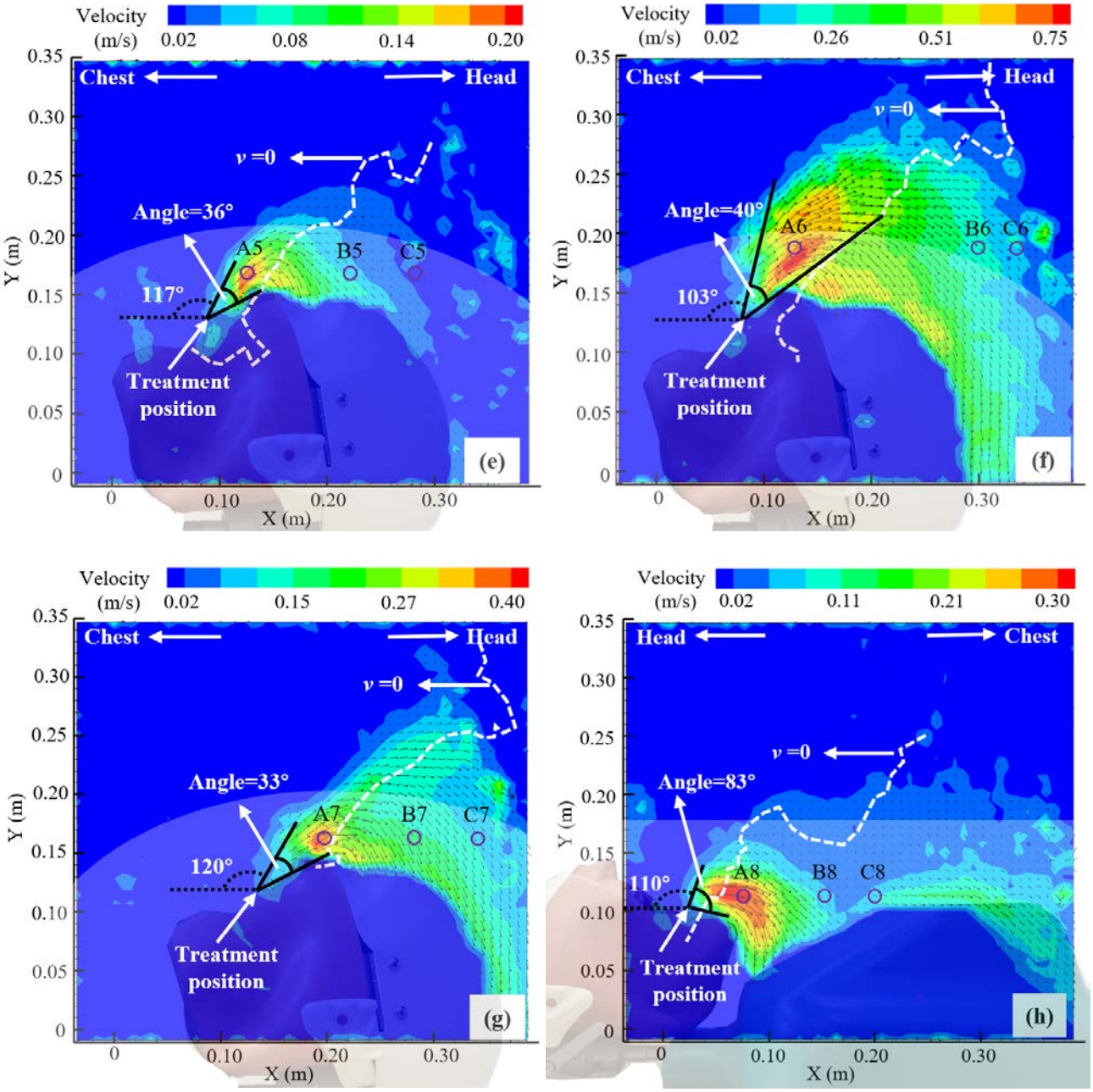
Velocity (m/s) 0.02 0.08 0.14 0.20
Chest
Head
v =0
Angle=36°
A5
B5
C5
117°
Treatment position
(e)
Velocity (m/s) 0.02 0.26 0.51 0.75
Chest
Head
v =0
Angle=40°
A6
B6
C6
103°
Treatment position
(f)
Velocity (m/s) 0.02 0.15 0.27 0.40
Chest
Head
v =0
Angle=33°
A7
B7
C7
120°
Treatment position
(g)
Velocity (m/s) 0.02 0.11 0.21 0.30
Head
Chest
v =0
Angle=83°
A8
B8
C8
110°
Treatment position
(h)
Y (m)
X (m)
0
0.05
0.10
0.15
0.20
0.25
0.30
0.35

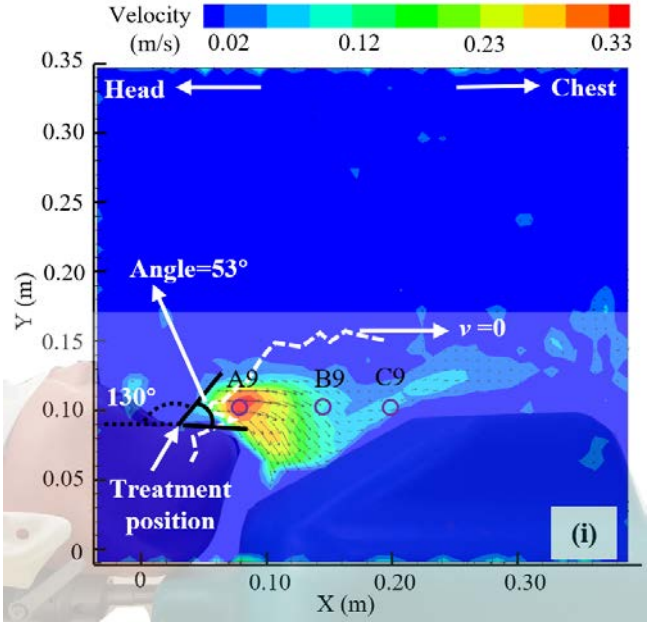

Figure 16 Time mean distribution of synthesis velocity of droplets generated by using the ultrasonic scaling instrument (from 200 samples) :(a) Case 1(30 ml/min; between 8th and 9th teeth), (b) Case 2 G0 (30 ml/min; between 8th and 9th teeth), (c) Case 2 G1 (30 ml/min; between 8th and 9th teeth), (d) Case 2 G2 (30 ml/min; between 8th and 9th teeth), (e) Case 3 (15 ml/min; between 8th and 9th teeth), (f) Case 4(50 ml/min; between 8th and 9th teeth), (g) Case 5 (30 ml/min; between 5th and 6th teeth), (h) Case 6 (30 ml/min; between 24th and 25th teeth), (i) Case 7 (30 ml/min; between 27th and 28th teeth).

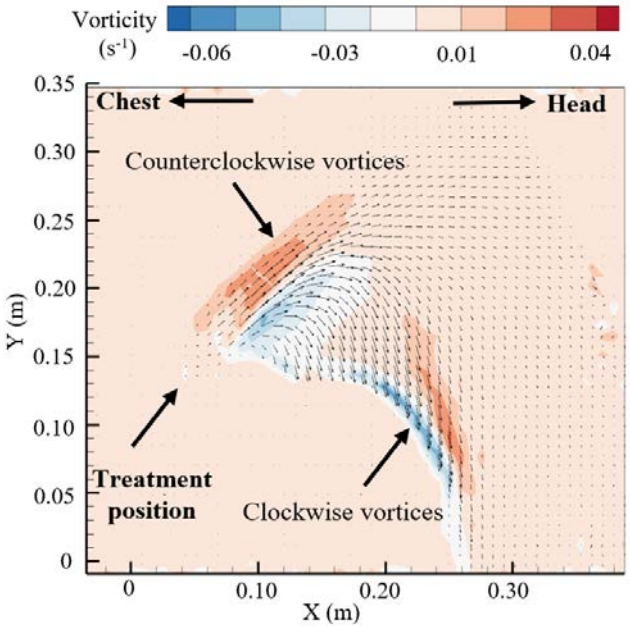

Figure 17 The time mean vorticity distribution of droplets during the process of ultrasonic scaling of Case 2 G0. Note that: Different cases have similar vorticity sizes and distribution characteristics.

Table 8 Coordinates of key points in the measured plane during the process of ultrasonic scaling.

Points	Case 1	Case 2 G0	Case 2 G1	Case 2 G2	Case 3	Case 4	Case 5	Case 6	Case 7
A	(0.14,0.19)	(0.12,0.20)	(0.15,0.18)	(0.16,0.17)	(0.13,0.17)	(0.13,0.18)	(0.20,0.16)	(0.08,0.11)	(0.08,0.10)
B	(0.22,0.19)	(0.22,0.20)	(0.25,0.18)	(0.27,0.17)	(0.22,0.17)	(0.30,0.18)	(0.28,0.16)	(0.14,0.11)	(0.15,0.10)
C	(0.30,0.19)	(0.30,0.20)	(0.32,0.18)	(0.33,0.17)	(0.28,0.17)	(0.34,0.18)	(0.34,0.16)	(0.20,0.11)	(0.20,0.10)

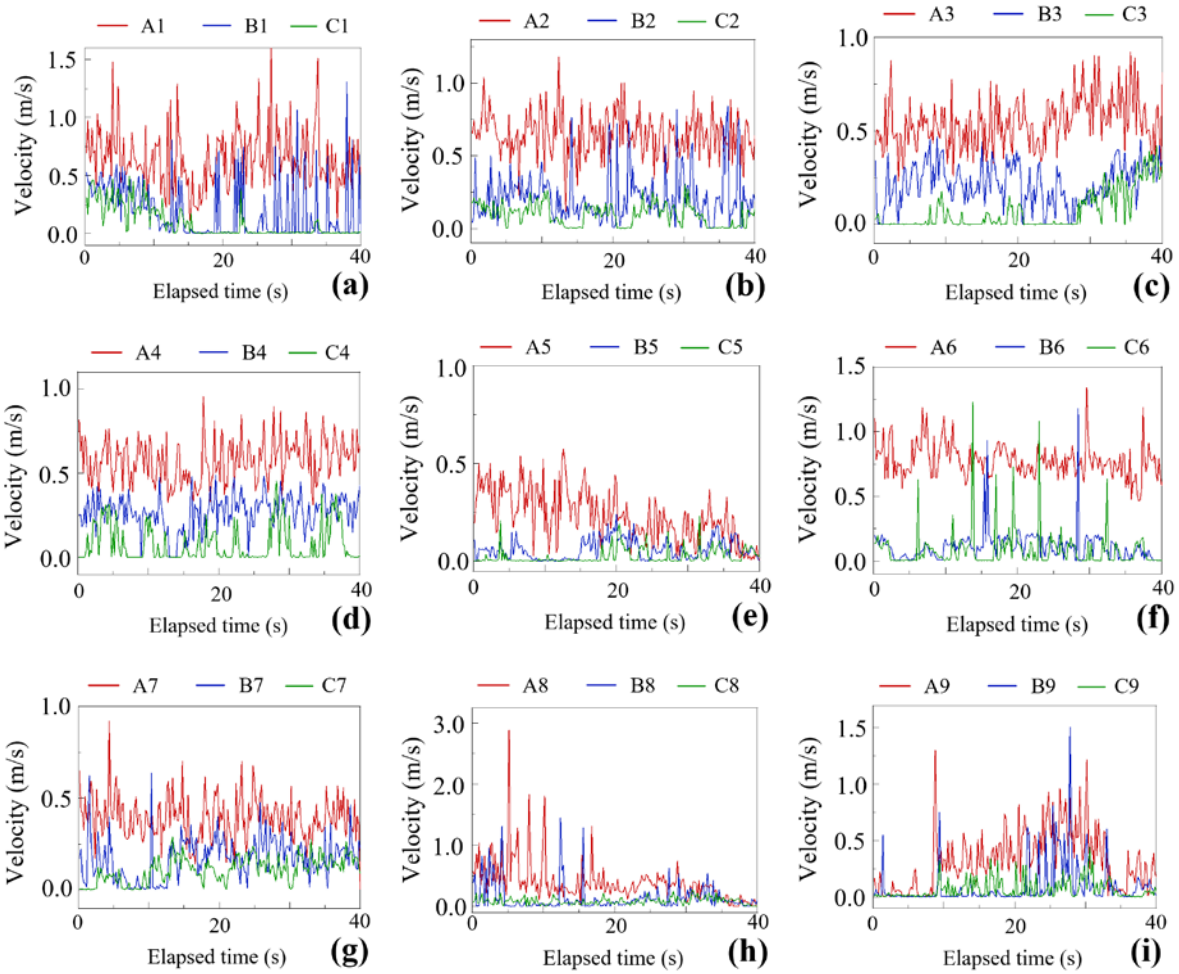

Figure 18 Instantaneous synthetized velocity distribution of droplets generated by using the ultrasonic scaling instrument at three typical points:(a) Case 1, (b) Case 2 G0, (c) Case 2 G1, (d) Case 2 G2, (e) Case 3, (f) Case 4, (g) Case 5, (h) Case 6, (i) Case 7.

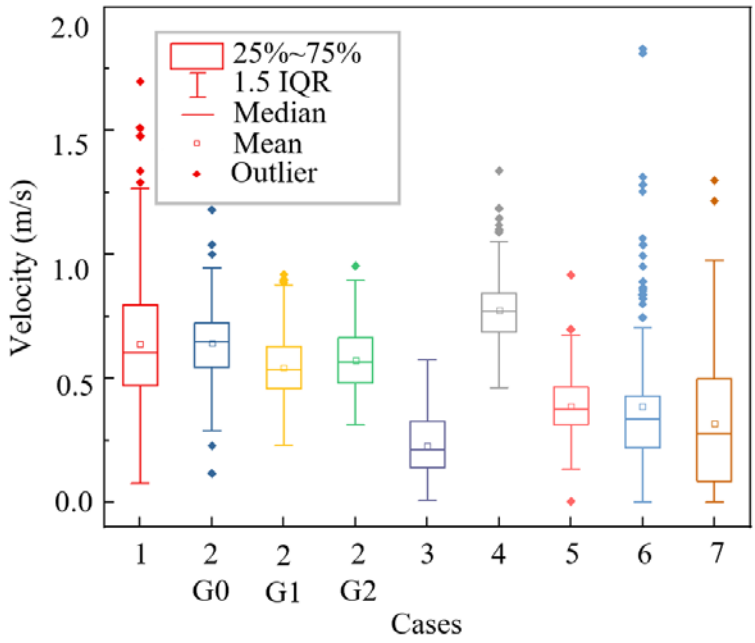

Figure 19 The synthetized velocity distribution of typical points (A) under different cases during the process of ultrasonic scaling.

Table 9 Key values in synthesis velocity distribution of droplets during the process of ultrasonic scaling.

Key values	Case 1	Case 2 G0	Case 2 G1	Case 2 G2	Case 3	Case 4	Case 5	Case 6	Case 7
Minimum	0.08	0.29	0.23	0.31	0.01	0.46	0.13	0.01	0.01
Maximum	1.27	0.95	0.88	0.89	0.57	1.05	0.67	0.70	0.98
Mean	0.61	0.64	0.54	0.57	0.22	0.77	0.37	0.34	0.27
Median	0.64	0.65	0.55	0.58	0.23	0. 78	0.38	0.39	0.32

References

[1] A. Bogdan, M. I. Buckett, D. A. Japuntich (2014). Nano-sized aerosol classification, collection and analysis–method development using dental composite materials. Journal of occupational and environmental hygiene, 11(7), 415-26.

[2] G. Schmalz, R. Hickel, K. L. Van Landuyt, et al. (2018). Scientific update on nanoparticles in dentistry. International dental journal, 68(5), 299–305.

[3] M. Syed, R. Chopra, V. Sachdev (2015). Allergic reactions to dental materials-A systematic review. Journal of clinical and diagnostic research, 9(10), ZE 04 – ZE 09.

[4] J. F. Chan, C. C. Yip, K. K. To, et al. (2020). Improved molecular diagnosis of COVID-19 by the novel, highly sensitive and specific COVID-19-RdRp/Hel real-time reverse transcription-PCR assay validated in vitro and with clinical specimens. Journal of clinical microbiology, 58(5).

[5] K. K. -W. To, O. T.-Y. Tsang, C. C.-Y. Yip, et al. (2020). Consistent detection of 2019 novel coronavirus in saliva. Clinical infectious diseases, 71(15), 841-843.

[6]R. Wolfel, V. Corman, W. Guggemos, et al. (2020). Virological assessment of hospitalized cases of coronavirus disease. Nature, 581, 465–469.

[7] A. L. Wyllie, J. Fournier, A. Casanovas-Massana, et al. (2020). Saliva is more sensitive for SARS-CoV-2 detection in COVID-19 patients than nasopharyngeal swabs. Medrxiv.

[8] M. A. Zoughool, Z. A. Shehri (2018). Injury and infection in dental clinics: risk factors and prevention. Toxicology and industrial health, 34(9), 609-619.

[9] D.J. Jia, J. Lee Baker, A. Rameau, et al. (2021). Simulation of a vacuum helmet to contain pathogen-bearing droplets in dental and otolaryngologic outpatient interventions. Physics of fluids, 33, 013307.

[10] T. Dbouk, D. Drikakis (2020). On respiratory droplets and face masks. Physics of fluids, 32(6), 063303.

[11] L. Bourouiba (2020). Turbulent gas clouds and respiratory pathogen emissions: Potential implications for reducing transmission of COVID-19. The journal of the American medical association, 323,1837–1838.

[12]Z. Ai, C. M. Mak, N. Gao, et al. (2020). Tracer gas is a suitable surrogate of exhaled droplet nuclei for studying airborne transmission in the built environment. Building simulation, 13, 489–496.

[13] S. Shetty, K. Sharath, S. Shenoy, et al. (2013). Compare the effcacy of two commercially available oralrinses in reducing viable bacterial count in dental aerosol produced during ultrasonic scaling when used as a preprocedural rinse. The journal of contemporary dental practice, 14(5), 848851.

[14] B. Retamal-Valdes, G. Soares, B. Stewart, et al. (2017). Effectiveness of a pre-procedural mouthwash in reducing bacteria in dental aerosols: randomized clinical trial. Brazilian oral research, 31,21.

[15] V. C. Marui, M. L. S. Souto, E.S. Rovai, et al. (2019). Efficacy of preprocedural oralrinses in the reduction of microorganisms in aerosol: a systematic review. Journal of America dental association, 150, 1015.

[16] T. V. Narayana, L. Mohanty, G. Sreenath, et al. (2016). Role of preprocedural rinse and high volume evacuator in reducing bacterial contamination in bioaerosols. Journal of oral and maxillofacial pathology, 20(1), 59-65.

[17] X. Xu, X. Chen, Q. Chen et al. (2020). Detection and analysis of the number of

bacterial colonies in the air of dental clinic during ultrasonic cleaning. Chinese journal of practical stomatology, 13(9), 551–554.

[18] B. Chanpong, M. Tang, A. Rosenczweig, et al. (2020). Aerosol-generating procedures and simulated cough in dental anesthesia. Anesthesia progress, 67(3),127–134.

[19] R. Holliday, J. R. Allison, C. C. Currie, et al. (2021). Evaluating contaminated dental aerosol and splatter in an open plan clinic environment: Implications for the COVID-19 pandemic. Journal of dentistry, 105, 103565.

[20] J. R. Allison, C. C. Currie, D. C. Edwards, et al. (2021). Evaluating aerosol and splatter following dental procedures: Addressing new challenges for oral health care and rehabilitation. Journal of oral rehabilitation, 48, 61–72.

[21] C. Zemouri, C. Volgenant, M. Buijs, et al. (2020). Dental aerosols: Microbial composition and spatial distribution. Journal of oral microbiology, 12(1), 1762040.

[22] J. L. Holloman, S. M. Mauriello, L. Pimenta, et al. (2015). Comparison of suction device with saliva ejector for aerosol and spatter reduction during ultrasonic scaling. Journal of the American dental association, 146(1), 27–33.

[23] P. Bernard (2021). Exposure of staff to aerosols and bioaerosols in a dental office. Building and environment, 187, 107388.

[24] C. Xing, S. Zhang, M. Bai, et al. (2021). Spatiotemporal distribution of aerosols generated by using powder jet handpieces in periodontal department. Sustainable cities and society, 75, 103353.

[25] GB/T1883-2002. (2002). Indoor Air Quality Standard. Beijing: Standards press of China.

[26] X. Li, M. C. Mak, K. W. Ma, et al. (2021). Evaluating flow-field and expelled droplets in the mock-up dental clinic during the COVID-19 pandemic. Physics of fluids 33, 047111.

[27] E. A. Haffner, M. Bagheri, J. E. Higham, et al. (2021). An experimental approach to analyze aerosol and splatter formations due to a dental procedure. Experiments in fluids, 62, 202.

[28] J. Plog, J. Wu, Y. J. Dias, et al. (2020). Reopening dentistry after COVID-19: Complete suppression of aerosolization in dental procedures by viscoelastic Medusa Gorgo. Physics of fluids, 32, 083111.

[29] Q. Ou, R.G. Placucci, J. Danielson, et al. (2021). Characterization and mitigation of aerosols and splatters from ultrasonic scalers. The journal of the American dental

association, 152(12), 981-990.
[30] P. Han, H. Li, L. J. Walsh, et al. (2021). Splatters and Aerosols Contamination in Dental Aerosol Generating Procedures. Applied science, 2021, 11(4), 1914.
[31] X. Cao, J. Liu, N. Jiang, et al. (2014). Particle image velocimetry measurement of indoor airflow field: A review of the technologies and applications. Energy and buildings, 69, 367–380.
[32] G. Zhou, J. Wang, R. Song, et al. (2022). Experimental study on droplet breakup and droplet particles diffusion of a pressure nozzle based on PIV. Chemical engineering science, 258, 31, 117737.
[33] A. Boillot, A.K. Prasad (1996). Prasad Optimization procedure for pulse separation in cross-correlation PIV. Experiments in fluids, 21, 87–93.
[34] P. Rosin (1933). The laws governing the fineness of powdered coal. Materials science, 7, 29-36.
[35] Z. Liu, G. Yao, Y. Li, et al. (2022). Bioaerosol distribution characteristics and potential SARS-CoV-2 infection risk in a multi-compartment dental clinic. Building and environment, 225, 109624.
[36] X. Li, C. M. Mak, Z. Ai, et al. (2023). Cross-infection risk assessment in dental clinic: Numerical investigation of emitted droplets during different atomization procedures. Journal of building engineering, 75, 106961.
[37] J. Komperda, A. Peyvan, D. Li, et al. (2021). Computer simulation of the SARS-CoV-2 contamination risk in a large dental clinic. Physics of fluids, 33, 033328.